Title: PTEX helps efficiently traffic haemoglobinases to the food vacuole in *Plasmodium falciparum*.

Thorey K. Jonsdottir[1,2,#a,b*], Brendan Elsworth[1,#c], Simon Cobbold[3,#d], Mikha Gabriela[1,4,#e], Sarah C. Charnaud[1,#f], Madeline G. Dans[1,#e], Molly Parkyn Schneider[1], Malcolm McConville[3], Hayley E. Bullen[1,2,†], Brendan S. Crabb[1,2,5,†] and Paul R. Gilson[1,2,†*]

[†]These authors contributed equally to this work

[1]Malaria Virulence and Drug Discovery Group, Burnet Institute, Melbourne, Australia

[2]Department of Immunology and Microbiology, University of Melbourne, Melbourne, Australia

[3]Department of Biochemistry and Molecular Biology, Bio21 Institute of Molecular Science and Biotechnology, University of Melbourne, Melbourne, Australia

[4]School of Medicine, Deakin University, Geelong, Australia

[5]Department of Immunology and Pathology, Monash University, Melbourne, Australia

Current addresses:

[#a]Department of Molecular Biology, Umeå University, Umeå, Sweden

[#b]The Laboratory for Molecular Infection Medicine Sweden (MIMS), Umeå, Sweden

[#c]Division of Emerging and Transfusion Transmitted Diseases, Office of Blood Research and Review, Center for Biologics Evaluation and Research, Food and Drug Administration, Silver Spring, MD, United States of America

[#d]Ubiquitin Signalling Division, Walter and Eliza Hall Institute, Melbourne, Australia

[#e]Infectious Diseases and Immune Defences Division, Walter and Eliza Hall Institute, Melbourne, Australia

[#f] Research for Health Department, World Health Organization, Geneva, Switzerland

*Corresponding authors: paul.gilson@burnet.edu.au and thorey.jonsdottir@umu.se

Abstract

A key element of *Plasmodium* biology and pathogenesis is the trafficking of ~10% of the parasite proteome into the host red blood cell (RBC) it infects. To cross the parasite-encasing parasitophorous vacuole membrane, exported proteins utilise a channel-containing protein complex termed the *Plasmodium* translocon of exported proteins (PTEX). PTEX is obligatory for parasite survival, both *in vitro* and *in vivo*, suggesting that at least some exported proteins have essential metabolic functions. However, to date only one essential PTEX-dependent process, the new permeability pathway, has been described. To identify other essential PTEX-dependant proteins/processes, we conditionally knocked down the expression of one of its core components, PTEX150, and examined which metabolic pathways were affected. Surprisingly, the food vacuole mediated process of haemoglobin (Hb) digestion was substantially perturbed by PTEX150 knockdown. Using a range of transgenic parasite lines and approaches, we show that two major Hb proteases; falcipain 2a and plasmepsin II, interact with PTEX core components, implicating the translocon's involvement in the trafficking of Hb proteases. We propose a model where these proteases are translocated into the PV via PTEX in order to reach the cytostome, located at the parasite periphery, prior to food vacuole entry. This work offers a another mechanistic explanation for why PTEX function is essential for growth of the parasite within its host RBC.

Author summary

Plasmodium falciparum is the causative agent of the most severe form of malaria in humans, where the symptoms of the disease are derived from the continuous asexual replication of the parasite within the human red blood cells (RBCs) it infects. To survive within this niche, the parasite exports hundreds of parasite effector proteins across the vacuole it resides within and into the RBC. About a quarter of the exported proteins appear to be essential during the blood stage but the functions of these proteins largely remain uncharacterised. Protein export is facilitated by an essential protein complex termed the *Plasmodium* translocon of exported proteins (PTEX). Conditional depletion of PTEX's core components results in rapid parasite death presumably because essential proteins do not reach their functional destination in the RBC and their associated metabolic functions cannot be performed. To uncover what these essential metabolic functions are we knocked down PTEX150, a core component of PTEX. Metabolic analysis of the knockdown parasites indicated that haemoglobin (Hb) digestion was inhibited resulting in a reduction of Hb derived peptides, which serve as an amino acid source for the parasite. We determined that knocking down HSP101, another PTEX core component, also disrupted the Hb digestion pathway. Furthermore, we provide evidence that reduction of Hb digestion might be due to the failure to efficiently deliver early acting Hb digesting proteases to the cytostome, a specialised location where vesicles of Hb are taken into the parasite. PTEX may therefore play a role in delivering Hb proteases to the cytostome.

Introduction

Malaria is a disease caused by *Plasmodium* parasites and transmitted to humans with the bite of an infected female *Anopheles* mosquito. Malaria remains a major health

and economic burden and it is estimated that 627,000 people died of malaria in 2020 (1). The clinical symptoms of malaria are derived from the asexual replicative stage of the parasite, which occurs within the red blood cells (RBCs) the parasite infects (2). During this stage the parasite invades the RBC whereupon it resides within a parasitophorous vacuole (PV); a membranous sac serving to occlude the parasite away from the RBC cytosol. The intracellular parasite is thus encased in two membranes, the parasite plasma membrane (PPM) and the parasitophorous vacuole membrane (PVM) (3). For survival within the infected RBC (iRBC), the parasite employs its own ATP-powered protein conduit at the PVM termed the *Plasmodium* translocon of exported proteins (PTEX) to export parasite effector proteins across the PVM and into the iRBC to establish essential host cell modifications (4-7).

PTEX is 1.6 MDa complex comprising three core proteins: Exported protein 2 (EXP2), PTEX150 and heat shock protein 101 (HSP101). Within this complex, EXP2 exists as a heptamer, which forms the PVM pore and binds directly to PTEX150, another hepatmer that serves as a stable channel for protein export. HSP101 exists as a hexamer and unfolds proteins, which it then extrudes through PTEX150 for transit through EXP2 and into the iRBC (4, 8-10). These three components cannot be knocked out in the human malaria parasite *P. falciparum* or the rodent malaria parasite *P. berghei* and conditional knockdown results in rapid parasite death and a block in protein export across the PVM, indicating PTEX mediated export is essential for parasite survival (4-7, 11-13).

Bioinformatic analyses have helped predict which proteins are likely exported based on the presence of a pentameric motif at their N-terminus called the *Plasmodium*

export element (PEXEL) motif and other export related features (14-18). Some exported proteins, however, lack the PEXEL motif, and are referred to as PEXEL negative exported proteins (PNEPs). Since PNEPs lack a signature export motif it is harder to predict their export (19). It is hypothesised that ~25% of the predicted exported proteome (exportome) is essential for *in vitro* blood stage growth but the essential functions remain unclear (20, 21). To date, only one essential function has been assigned to exported proteins, the establishment of the new permeability pathways (NPPs) at the iRBC surface, which help import essential nutrients from the surrounding blood plasma (22-27). However, most exported protein functions identified are not essential for *in vitro* growth and contribute to iRBC rigidity, virulence and immune evasion (28-30).

Here we conditionally knocked down one of PTEX's core components, PTEX150, and used metabolomics to identify biological processes affected when PTEX's function is perturbed and thereby the potential function(s) of the essential exportome. We initially anticipated a relative reduction in the levels of molecules known to enter the iRBC via the NPPs but instead discovered an unexpected link between haemoglobin (Hb) digestion and PTEX function. To strengthen this finding, we also observed an association of two major Hb proteases, falcipain 2a (FP2a) and plasmepsin II (PM II) with PTEX. Overall, the data provided in this study suggests that PTEX core components help with efficient trafficking of Hb proteases within the PV space *en route* to the food vacuole where Hb digestion occurs.

Results

2.1 Conditional knockdown of PTEX150 reduces the level of digested Hb.

To perturb the function of one of PTEX's principal components, we used a previously established parasite line where PTEX150 was appended with a triple haemagglutinin (HA) protein tag and a *glmS* riboswitch to conditionally knockdown PTEX150 in the presence of glucosamine (GlcN) (6, 31). Metabolomic analyses were performed on 18, 24 and 30-h post invasion (hpi) parasites synchronised to a 4 h window one cell cycle after the addition of 0.15 mM or 1 mM GlcN to induce knockdown of PTEX150 expression (Fig 1A).

Analysis of resultant data revealed that glycolysis and nucleotide metabolism was perturbed in PTEX150 knockdown parasites, indicating cellular homeostasis was dysregulated (S1 Table). This was predominantly observed in parasites 30-hpi, a treatment time at which the PTEX150 knockdown parasites are known to stall (6). These effects are therefore most likely a result of parasite growth arrest rather than a direct involvement of PTEX in these pathways (S1 Table).

The data also revealed that PTEX150 knockdown resulted in a noticeably lower abundance of Hb peptides when compared to untreated samples, indicating that Hb digestion was reduced in these parasites (Fig 1A, S1A Fig, S1 Table). The largest difference in Hb peptides abundance was observed at 24-hpi and 30-hpi in parasites treated with 1 mM GlcN (Fig 1A). However, unlike for glycolysis and nucleotide metabolism, this effect was also observed in parasites treated with 0.15 mM GlcN, which does not significantly affect parasite growth (Fig 1A, S1A Fig) (6). Therefore, reduction of digested Hb is likely due to PTEX150 knockdown and not due to a defect in overall parasite growth. In further support of this, a moderate decrease in certain

Hb peptides was also observed at 18-hpi and a noticeable decrease in 24-hpi parasites treated with either 0.15 or 1 mM GlcN, prior to when growth stalls due to PTEX150 knockdown (Fig 1A). Overall, these data indicate that knockdown of PTEX150 specifically reduces Hb digestion.

To corroborate these findings, the experiment was repeated using a single time point and a 3D7 wild-type (WT) parasite control to monitor any effects caused by the GlcN treatment itself on Hb peptide abundance. The parasites were synchronised and GlcN-treated as before using a single time point (24-hpi). This time point was chosen because the majority of Hb digestion occurs 18 – 32-hpi (32, 33). As previously observed, the most dramatic metabolic differences between the lines following PTEX150 knockdown are in the levels of Hb peptides (Fig 1B, S1B Fig, S1 Table). Specifically, the 3D7 WT parasites showed a slight decrease in some Hb peptides when treated with GlcN, but the reduction observed for PTEX150-HA*glmS* expressing parasites was much greater (Fig 1, S1 Fig). Collectively these data indicate that PTEX likely plays a role in the Hb digestion pathway.

2.2 Establishing a falcipain 2a knockdown line as a positive control for disturbance to Hb digestion.

It was not immediately obvious how knockdown of PTEX reduces Hb peptides and so we postulated that PTEX could either be involved in the uptake of Hb or involved in the trafficking of the early acting falcipain and plasmepsin Hb proteases to the cytostome *en route* to the food vacuole / digestive vacuole (34-36). The cytostome is an invagination of both the PPM and the PVM from which Hb containing vesicles

bud off for transport to the food vacuole where the majority of Hb digestion occurs (37, 38). Uptake of Hb and digestion are both important for parasite survival, providing both amino acids (aa) and space for the growing parasite (33, 39-41). Falcipain 2a (FP2a) is one of the early acting Hb proteases (42-44) and due to this, it was chosen for this study to determine if knocking down FP2a expression would mimic the effects observed for PTEX150 knockdown. We appended the C-terminus of the *fp2a* gene (PF3D7_1115700) with a single HA-tag and the *glmS* riboswitch using the CRISPR/Cas9 approach (S2A Fig). C-terminal tagging has not previously been found to affect its trafficking or function (34-36). Furthermore, FP2a is not individually essential for *in vitro* growth (45, 46), therefore knocking it down would not be expected to severely reduce parasite growth.

Correct integration of the tag to the *fp2a* locus was confirmed via PCR (S2B Fig) and western blotting was used to confirm the presence of FP2a-HA*glmS*, where both pro- (54 kDa) and mature (27 kDa) forms of the protease were observed as has been reported previously (43, 47) (S2C Fig). To investigate the level of knockdown, FP2a-HA*glmS* trophozoite stage parasites were treated with increasing concentrations of GlcN for one cell cycle and >90% protein knockdown was observed by western blotting (S2C Fig). Immunofluorescence assays (IFAs) were then used to determine the localisation of FP2a-HA*glmS* within iRBC where it showed diffuse localisation in the parasite cytoplasm (S2D Fig), often with concentrated puncta around the parasite surface, possibly representing the cytostome as has been previously observed (34, 36, 48) (S2D Fig, white arrows). While green fluorescent protein (GFP) tagged FP2a is shown to concentrate in the food vacuole, FP2a-HA*glmS* was found throughout the parasite cytoplasm as previously observed with a native FP2a antibody (34). This is

not entirely unexpected, as previous reports of a HA-tagged food vacuole protein, lipocalin (PF3D7_0925900), showed that the HA-tag is degraded upon food vacuole entry (49). The HA-tag of our FP2a-HA*glmS* could therefore also be degraded and not easily detectable inside the food vacuole by IFA.

To assess parasite growth upon FP2a-HA*glmS* knockdown, multi-cycle growth assays were conducted on both 3D7 WT and FP2a-HA*glmS* parasites. Trophozoite stage parasites were treated with increasing concentrations of GlcN over three consecutive cell cycles and harvested at each cycle to measure lactate dehydrogenase (LDH) activity as a proxy for parasite growth (50, 51). As expected, there was no growth reduction observed in the FP2a-HA*glmS* knockdown parasites relative to untreated (0 mM GlcN) parasites or the 3D7 WT control which concurs with previous FP2a knockout studies (52) (S2E Fig).

2.3 Knocking down PTEX's core components, PTEX150 and HSP101, causes a build-up of full-length Hb inside the parasite.

To determine if reduced Hb peptides upon PTEX150 knockdown was due to either reduced Hb uptake, or reduced Hb digestion, we completed western blotting on both the PTEX150-HA*glmS* line, and an additional line in which the core PTEX component HSP101 was similarly tagged (HSP101-HA*glmS*) (53). As a control for Hb digestion we utilised the FP2a-HA*glmS* parasite line, as well as 3D7 WT parasites as a negative control.

223 To complete these assays, tightly synchronised trophozoite stage parasites (~24-hpi)
224 were treated with 0, 0.15 or 1 mM GlcN for one cell cycle and the RBCs were
225 subsequently lysed in 0.09% saponin to remove RBC Hb. The parasite pellets were
226 washed extensively in PBS to remove Hb contamination prior to western blotting (Fig
227 2A and 2B). As expected, the 3D7 WT control showed minimal changes in Hb levels,
228 whereas following knockdown of PTEX150-HA*glmS*, HSP101-HA*glmS* or FP2a-
229 HA*glmS*, full-length Hb was found to accumulate inside the parasite. This
230 accumulation was found to be inversely proportional to the level of knockdown; a
231 reduction in PTEX150-HA*glmS*, HSP101-HA*glmS* or FP2a-HA*glmS* proteins was
232 associated with an increase in undigested Hb inside the parasite (Fig 2A and 2B).
233 Importantly, this effect was not due to an overall growth defect in the *glmS* lines upon
234 protein knockdown as build-up of full-length Hb was also detected at low GlcN
235 concentrations (0.15 mM) at which parasite growth of FP2a-HA*glmS* (S2E Fig) and
236 PTEX150-HA*glmS* (6) was not substantially perturbed. Although the Hb-build up was
237 only found to be significant for the FP2a-HA*glmS* parasites when comparing % Hb
238 build-up compared to untreated, both PTEX150-HA*glmS* and HSP101-HA*glmS*
239 showed a strong trend for Hb-build up with increased protein knockdown. We were
240 not able to establish a strong knockdown for either PTEX150-HA*glmS* or HSP101-
241 HA*glmS*, which might be why we don't observe a significant increase in full-length
242 Hb inside. FP2a was almost completely knocked down which is likely why we were
243 able to achieve statistically significant results. We therefore also performed a simple
244 linear regression analysis, where all three parasite lines (PTEX150-HA*glmS*, HSP101-
245 HA*glmS* and FP2a-HA*glmS*) showed significant regression slope for Hb build-up
246 when protein expression was reduced (S3A Fig).
247

To complement our results, we completed IFAs on saponin-lysed parasites probed with antibodies against full-length Hb (Fig 2C, 2D and 2E). Following 1 mM GlcN treatment of PTEX150-HA*glmS* parasites as described above, full-length Hb was also observed accumulating within the parasite, independent of parasite size, confirming previous results (Fig 2C, 2D and 2E).

As Hb is digested by the parasite, toxic by-products from this process are sequestered as haemozoin crystals, which can be observed by light microscopy. In the absence of Hb digestion, these crystals are therefore not formed (54). We investigated the presence of haemozoin crystals in our PTEX knockdown lines. Specifically, either PTEX150-HA*glmS* or HSP101-HA*glmS* were treated for one cell cycle ± 2.5 mM GlcN to reduce respective protein expression (S3B, S3C and S3D Fig). 2.5 mM GlcN treatment was used because it produces the largest degree of knockdown for *glmS*-tagged proteins without noticeably reducing the growth of non-tagged parasites (6, 53). Both PTEX150-HA*glmS* and HSP101-HA*glmS* knockdown resulted in significantly less haemozoin crystal formation (S3B and S3C Fig) indicating less Hb was being digested which concurs with western blotting and IFA data above (Fig 2). At this level of GlcN, we did observe a significant reduction in parasite size for the PTEX150-HA*glmS* parasites but not for HSP101-HA*glmS* (S3D Fig). Collectively these data demonstrate that upon modest knockdown of the PTEX components PTEX150-HA*glmS* and HSP101-HA*glmS*, parasites still take up Hb. However, the parasites are unable to properly digest Hb indicating that PTEX may be involved in the trafficking of proteases involved in the degradation of Hb, and likely not the process by which the Hb is taken into the parasite.

2.4 Generation of FP2a trappable reporter cargoes to investigate FP2a relationship with PTEX.

Next, we sought to better understand the relationship between PTEX and Hb digestion. To this end, we generated a series of FP2a reporter constructs to investigate the reporters' trafficking and interaction with PTEX *en route* to the food vacuole as the protease is thought to traffic to the food vacuole via the cytostome at the PPM/PVM interface (34, 35, 43). Three FP2a reporters of differing lengths were generated, all appended to a nanoluciferase (Nluc) ultra-bright bioluminescence reporter (55), murine dihydrofolate reductase domain (DH) and a triple FLAG (FL) epitope tag. The initial two constructs included the first 120 or 190 aa of FP2a, here referred to as "120 aa" and "190 aa", respectively (Fig 3A). Previous truncation studies demonstrated that the first 105 aa of FP2a are sufficient for its trafficking to the food vacuole (35), however a construct containing the first 120 aa was more efficiently trafficked to the food vacuole which is why this length was chosen here (34, 35). The longer 190 aa version was made to investigate if an N-terminus longer than 120 aa would provide an even more efficient PPM extraction as this has been shown to be important for exported transmembrane (TM) domain proteins (56). A third reporter was generated as a negative control and contained the N-terminal trafficking region of FP2a but lacked the N-terminal TM domain (Fig 3A) required for entry into the secretory pathway (34, 35) and subsequent trafficking to the food vacuole. This reporter is referred to as "NT" throughout the text (Fig 3A).

By adding an antifolate ligand such as WR99210 (WR) we can stabilise the globular domain of DH and thereby inhibit the reporter proteins from unfolding. The DH domain has been previously utilised to study both mitochondrial protein import (57)

297 and protein export in malaria parasites (56, 58, 59). PTEX requires cargo to be
298 unfolded prior to export (58) and therefore if FP2a is trafficked via PTEX, the 120
299 and 190 aa reporters should become trapped in PTEX when inhibited from being
300 unfolded via addition of WR as previously observed for exported protein reporters
301 (56, 59).
302
303 All reporters were episomally expressed in the HSP101-HA*glmS* background, under
304 the *ef1a* promoter (Fig 3A). They were successfully detected by western blotting,
305 where they migrated at the expected sizes (Fig 3B). Additionally, IFA analysis
306 confirmed that the 120 and 190 aa reporters were trafficked to the food vacuole where
307 they co-localised with the haemozoin crystals whilst the NT reporter displayed a
308 diffuse signal within the parasite cytoplasm, as expected (Fig 3C). The 190 aa reporter
309 appeared to be more concentrated at the food vacuole than the 120 aa reporter
310 indicating that the longer N-terminus could enable more efficient trafficking to the
311 food vacuole (Fig 3C). Brefeldin A (BFA), which blocks protein secretion from the
312 ER to the Golgi (60, 61), was also used to confirm that the reporters were secreted
313 from the ER as happens for the native protease (34, 35). In the presence of BFA the
314 120 and 190 aa reporters were retained within the ER whilst no changes were
315 observed for the distribution of the NT reporter as expected (Fig 3D). Overall, these
316 data confirm that the reporters are expressed and appropriate for use in subsequent
317 PTEX trapping experiments.

318 **2.5 The FP2a 120 aa reporter displays increased co-localisation with EXP2 when**
319 **inhibited from unfolding.**

320 To determine if FP2a associates with PTEX, the 120 aa, 190 aa and NT reporters were
321 trapped using WR and IFAs were performed to detect co-localisation with PTEX
322 components at the PVM. Tightly synchronised (4 h window) ring stage parasite
323 cultures were treated ± 10 nM WR and harvested as trophozoites (24-28-hpi) for
324 IFA. Rabbit anti-Nluc was used to visualise the FP2a reporters and mouse anti-EXP2
325 served as both a PTEX and PVM marker (Fig 4A). The 120 and 190 aa reporters
326 displayed some labelling around the parasite surface/PVM, which was expected as
327 early acting Hb proteases are known to traffic there for loading into the cytostome
328 prior to delivery to the food vacuole (34-36). To quantify the co-localisation of
329 reporters with EXP2 ± WR, Pearson's coefficients of the proteins were measured
330 (Fig 4B). The 120 aa co-localised significantly more with EXP2 when treated with
331 WR indicating that more cargo was trapped at the parasite periphery when rendered
332 unfoldable and therefore potentially trapped in PTEX (Fig 4A and 4B). However, the
333 190 aa and NT reporters did not show a significant difference ± WR treatment (Fig
334 4A and 4B). Since the 120 and 190 aa reporters are identical except for their length, it
335 is likely that length is influencing trapping efficiency and that shorter cargo is more
336 easily trapped (discussed in later sections).
337
338 Interestingly, even though the 120 aa cargo co-localised with EXP2, it was never
339 observed inside EXP2 loops (Fig 4A, white arrows) which we commonly observe for
340 the exported reporter Hyp1-Nluc-DH upon WR trapping (59, 62). These loops are
341 thought to represent accumulated trapped cargo unable to be transported by the PTEX
342 complex at the PVM (59). The absence of the FP2a reporter cargo from these loops

could indicate that it might not be trapped at the PVM, but instead at the PPM. We sought to further investigate the putative interaction between PTEX and FP2a using co-immunoprecipitation assays (Co-IPs).

2.6 Both the 120 aa and the 190 aa reporters associate with PTEX core components, but this association is diminished when reporters are inhibited from unfolding.

To investigate the interaction between HSP101 and FP2a, Co-IPs were performed with the three FP2a reporters (NT, 120 aa, 190 aa). We also employed an exported protein reporter, Hyp1-Nluc-DH-FL or "Hyp1", as a positive control for PTEX interaction (53). Synchronised ring stage parasites were treated ± 10 nM WR and trophozoite stage iRBCs (~28-32-hpi) were isolated from uninfected RBCs (uRBCs) by magnet purification. This time point was chosen because it was when the FP2a and Hyp1 reporter proteins were optimally expressed with less degradation (S4 Fig) (53). Parasite pellets were lysed in modified RIPA buffer and the resultant lysate was incubated with anti-HA agarose beads to immunoprecipitate (IP) HSP101-HA*glmS* and its interacting proteins for visualisation by western blotting (Fig 5A).

As expected, the Hyp1 reporter showed an increased association with HSP101 when treated with WR reflective of the folded cargo becoming trapped in PTEX under these conditions (53, 59) (Fig 5A, lanes 9 and 10, 5B and 5C). The NT reporter showed a minimal level of association with HSP101 (Fig 5A, lanes 11 and 12, 5B and 5C) as expected. Importantly, both the 120 and 190 aa reporters showed an enhanced association with HSP101 in the absence of WR, demonstrating that FP2a does indeed

interact with HSP101 (Fig 5A, lanes 13 – 16, 5B and 5C). It should be noted that a marked difference was observed between the retention of the 120 and 190 aa reporters (Fig 5A lanes 13 and 14 vs. lanes 15 and 16) with HSP101, whereby substantially more of the 120 aa reporter was bound by HSP101. This concurs with the greater trapping efficiency of the 120 aa reporter at the parasite periphery with EXP2 as visualised by IFA (Fig 4).

It was anticipated that in the presence of WR, the reporters would be more strongly associated with HSP101 if they were trapped in PVM-resident PTEX, but instead the association of the reporters with HSP101 was reduced (Fig 5A, lanes 13 – 16, 5B and 5C). These data therefore imply that WR treated 120 and 190 aa reporter proteins might in fact be trapped in the PPM prior to PTEX association in the PV as has been observed for PNEPs (56). This explains why we did not observe the FP2a reporters in PVM loops by IFA (59) as mentioned above.

Association of the FP2a reporters was also confirmed for PTEX150 and EXP2 by Co-IP using either rabbit anti-PTEX150 (r942) (S5A Fig) or rabbit anti-EXP2 (r1167) (S5B Fig) antibodies. PTEX150 showed a similar association with FP2a cargo as HSP101 (S5A Fig, lanes 13 – 16) and a weak association was observed for the cargoes with EXP2 (S5B Fig, lanes 13 – 16). Densitometry measurements showed a similar trend for the association of Hyp1 and FP2a reporters with both PTEX150 and EXP2 when compared with HSP101 IPs (S6 Fig). Overall, these assays helped to confirm that FP2a interacts with all PTEX core components, as was suggested by our metabolomics and Hb digestion/build-up assays.

391 **2.7 The FP2a 120 aa reporter becomes trapped at the PPM with the N-terminus**
392 **facing into the PV compartment when inhibited from unfolding.**

393 Given that the 120 aa reporter cargo displayed an increased co-localisation by IFA
394 with EXP2 when inhibited from unfolding (Fig 4B) but showed reduced association
395 with PTEX components when trapped with WR (Fig 5 and S5 Fig), we utilised
396 proteinase K protection assays to determine which iRBC compartment the reporter
397 was being trapped in. For the assay, synchronised ring stage parasites were treated ±
398 10 nM WR, prior to harvesting at the trophozoite stage (~24-hpi) via magnet
399 purification. Isolated trophozoite-containing RBCs were treated with equinatoxin-II
400 (EQT) to form pores in the iRBC membrane (63) and release soluble exported
401 proteins (Fig 6A, lanes 1 and 6, SN). The subsequent iRBC pellet was then divided
402 into four fractions that were untreated, treated with proteinase K, or subjected to
403 differential lysis conditions and proteinase K treatment. Saponin was used to lyse the
404 parasite's PVM, releasing the PV contents (Fig 6A, lanes 4 and 9) and Triton X-100
405 (TX-100) was used to lyse all membranes (Fig 6A, lanes 5 and 10). Specific
406 antibodies were then used as markers for each lysed compartment, where GBP130
407 was used as a soluble exported protein marker (59, 64), SERA5 as a soluble PV
408 marker (65) and GAPDH as a marker of the parasite cytoplasm.
409
410 By analysing the distribution of FP2a bands across all treatments, it was possible to
411 infer the orientation and localisation of the 120 aa reporter protein. Firstly, the
412 reporter protein was not degraded in the presence of PBS and proteinase K, indicating
413 no part of the reporter resided within the iRBC cytoplasm, which concurs with our
414 IFA data (Figs 6A, lanes 3 and 8 and 4A). Concordantly, when the parasites were
415 treated with saponin and proteinase K, the FP2a reporter migrated 3.8 kDa smaller

than the full-length reporter (Fig 6A, lanes 4 and 9). This 3.8 kDa fragment is proportional to the segment of the reporter protein that precedes the N-terminal TM domain (4 kDa) suggesting that FP2a is oriented with its N-terminus facing into the PV lumen, and the C-terminus is in the parasite cytoplasm (Fig 6C). The FP2a reporter was completely degraded in the presence of TX-100 indicating that the parasite membranes were completely permeabilised (Fig 6A, lanes 5 and 10). GAPDH was not degraded, likely because the protein is highly abundant and proteolytically resistant.

Following WR treatment, the FP2a reporter parasites that were lysed with saponin and treated with proteinase K revealed that the reporter was more resistant to degradation than it was in the absence of WR (Fig 6A and 6B, lanes 3 and 4 vs. lanes 8 and 9) suggesting that FP2a needs to be unfolded before crossing the PPM and entering the PV compartment. This demonstrates that the WR trapping occurs at the PPM interface prior to PTEX association within the PV, which agrees with our IP data where FP2a shows less interaction with PTEX components when treated with WR (Fig 5 and S5 Fig).

2.8 PTEX150 co-precipitates native plasmepsin II Hb protease and PTEX150 knockdown affects protease trafficking.

To study the relationship between PTEX and a native Hb protease, we tagged the early acting Hb protease plasmepsin II (PM II, PF3D7_1408000) with mScarlet as described for FP2a-HA*glmS* above (S7A Fig), however, the background line used for transfection of this line was PTEX150-HA*glmS*. Integration was confirmed by PCR (S7B Fig). A single band of 75 kDa was detected for PM II-mScarlet by western blotting, where the tag accounted for approximately 27 kDa (Fig 7A). This agrees

441 with previously published results where only the pro form of the protease was
442 detected and not the mature cleaved protease (66). Live cell microscopy confirmed
443 the localisation of PM II-mScarlet during ring and trophozoite stage, where the
444 protease co-localised with the haemozion crystals (Fig 7B, white dotted line) as
445 expected. To determine if PTEX is involved in PM II trafficking, we knocked down
446 PTEX150-HA*glmS* expression at the trophozoite stage and harvested cells for
447 microscopy at the following late ring stage (~20-hpi). We observed a significant
448 accumulation of PM II-mScarlet at the parasite periphery when PTEX150 was
449 knocked down (crescent/circle) compared to a peripheral 'dot' when PTEX150 was
450 normally expressed (Fig 7C and 7D). While this is qualitative evidence for a role for
451 PTEX150 in PM II-mScarlet trafficking to the food vacuole, some observations could
452 merely represent PM II-mScarlet during its normal trafficking to the cytostome via
453 the parasite periphery. To support that our observations are indeed due to an
454 interaction with PTEX150, we targeted PTEX150-HA*glmS* for IP using anti-HA
455 agarose beads as previously described. A strong association was seen between
456 PTEX150-HA*glmS* and PM II-mScarlet (Fig 7E). Positive control antibodies against
457 HSP101 and EXP2 also revealed that they too associated with PTEX150 as expected,
458 while rabbit anti-GAPDH was used as a negative control and showed no association
459 (Fig 7E). 3D7 WT parasites were used to detect any non-specific antibody binding in
460 the assay and showed no interaction with PTEX150 or other PTEX components.
461 Overall, this assay confirmed a specific association between PTEX and a native Hb
462 protease (PM II-mScarlet) and agrees with our FP2a reporter data.
463

464 **Discussion**

This study sought to elucidate why PTEX is essential by determining which metabolic pathways were perturbed due to the failure to export proteins into the iRBC compartment when the protein components of PTEX were knocked down. Hundreds of parasite proteins are exported into the iRBC, but we do not know what most of these proteins do and why some of them are essential. Metabolomic analyses revealed that knockdown of PTEX150 caused a slight dysregulation of some metabolite levels, for example those involved in glycolysis and nucleotide metabolism, however this was also observed in the 3D7 WT control indicating a non-specific effect from the GlcN treatment. The only clearly defined effect of PTEX150 knockdown was upon Hb digestion, possibly linking the PTEX machinery to this essential catabolic process that provides the parasite with amino acids and helps maintain osmotic stability of the iRBC (33, 39-41). Using several approaches, we were able to determine a physical connection between PTEX and two major early acting Hb proteases, FP2a and PM II. It is possible that these Hb proteases might rely on PTEX components as they transit via the PPM *en route* to the cytostome (34-36).

Modest knockdown of PTEX150-HA*glmS* with 1 mM GlcN reduces PTEX150-HA*glmS* expression to ~60% of normal levels (in our study) and arrests growth at the late ring / early trophozoite stage in the cycle following addition of GlcN (6). As the degree of growth inhibition would also likely produce many metabolic defects, we also used 0.15 mM GlcN, which does not arrest parasite growth (6). This treatment also resulted in a reduction in Hb digestive peptides and western blotting and microscopy analysis demonstrated the reduction was likely due to diminished capacity to digest Hb rather than a defect in total Hb uptake. This contradicts results presented in a recent study by Gupta *et al*., where they observed less Hb uptake in

490 HSP101 knockdown parasites (67). Their study was however performed differently to
491 ours whereby HSP101 expression was knocked down from late trophozoite stage of
492 the first cycle to the early schizont stage of the next cycle (42-44-hpi). This could
493 result in the HSP101 knockdown parasites stalling at the early trophozoite stage of the
494 second cycle and therefore not being able to take up as much Hb as the untreated
495 control parasites which had continued growing and transitioned into to the schizont
496 stage. This trophozoite stalling effect due to functional inactivation of HSP101 has
497 been previously noted using the same HSP101 knockdown line (5).
498
499 To determine if PTEX knockdown was inhibiting the delivery of Hb proteases to
500 cytostomal vesicles we utilised FP2a reporter cargo constructs, which allowed us to
501 study the interactions between PTEX and this early acting Hb protease. The FP2a 120
502 aa and 190 aa reporters were directly co-precipitated with PTEX core components,
503 although much stronger with HSP101 and PTEX150 than EXP2. If the N-terminus of
504 the FP2a reporter that was poking into the PV (34 aa) was interacting with the PTEX
505 complex, it likely associates more with HSP101 and PTEX150 than EXP2, which is
506 further away (Fig 8). The slightly weaker association with EXP2, that was also
507 observed for the positive control Hyp1, could be due to IP efficiency. EXP2 has a
508 dual function; as a channel in the PTEX complex and as a nutrient channel on the
509 PVM (13, 68). This dual function could therefore influence the co-IP of EXP2 with
510 FP2a and Hyp1, as the pool of nutrient related EXP2 is not associated with PTEX
511 functioning. Importantly, each assay co-precipitated the other members of the PTEX
512 suggesting involvement of the full PTEX complex in protease binding (Fig 5 and S5
513 Fig) and a similar trend was observed for HSP101, PTEX150 and EXP2 IPs with
514 reporter cargoes (Fig 5B, 5C and S6A and S6B Fig). Importantly, this association was

515 also observed for a native early acting Hb protease, PM II, suggesting PTEX's
516 interaction with FP2a reporters reflected genuine trafficking interactions (Fig 7E). It
517 should be noted that conditionally inhibiting the function of HSP101 did not reduce
518 the proteolytic processing of native PM II (5) that normally occurs in the food vacuole
519 facilitated via FP2 and FP3 (69). Despite the knockdown of PTEX, some Hb peptides
520 were still produced and some haemozoin crystals did form. This indicates that
521 although PTEX was not essential for the trafficking of PM II (5), the translocon might
522 rather be important for efficient the delivery of Hb proteases to the cytostome.
523 However, given the modest level of knockdown achieved in this study the remaining
524 levels of PTEX expression could be sufficient to sustain protease trafficking and Hb
525 digestion. Although reduction in Hb digestion following PTEX knockdown probably
526 contributes to some growth arrest, the dysregulation of other metabolic pathways
527 might also play a greater role in reducing parasite growth, however, our analysis does
528 not indicate what these other pathways are.
529
530 As FP2a has been shown to traffic to the cytostomal vesicles via the parasite
531 periphery (34, 35) we investigated if PTEX may associate with the FP2a reporters at
532 the PPM. Here we demonstrated that the FP2a reporters likely need to be unfolded
533 prior to crossing the PPM, like exported proteins containing TM domains (10, 56, 70).
534 We showed this by appending an inducibly unfoldable DH domain to the reporters,
535 which in its unfoldable form was more strongly localised to the parasite periphery.
536 Our proteinase K protection assays further indicated the direction of insertion into the
537 PPM likely followed an N- to C-terminal direction. Immunoprecipitation assays
538 additionally showed that PTEX was in contact with the 120 aa and 190 aa FP2a
539 reporters and with the native PM II protein, suggesting PTEX could help extract these

proteins into the PV lumen. HSP101 has previously been suggested to facilitate the extraction of TM exported proteins from the PPM (71). An explanation as to how these proteases are trafficked to the cytostome via PTEX is that they are transferred into the PVM via PTEX, which is anchored to the PVM via EXP2, and then incorporated into the innermost membrane of the cytostomal vesicles. Although this is an attractive explanation for how PTEX assists Hb proteases to enter the cytostome, further experiments did not strongly support this scenario and PTEX does not have a lateral gate to facilitate the transfer of proteins to the PVM (9, 72, 73) (Fig 8, red x symbol).

Rather from our data it appears that the Hb proteases are not translocated through PTEX into the PVM since the FP2a reporters containing the DH domain did not co-localise to the PVM loops with EXP2 in the presence of WR as has been shown previously for export-blocked PEXEL-DH reporter proteins (59). Secondly, the 120 aa FP2a reporter was protected from protease degradation when the iRBC was permeabilised with EQT but not when the PVM was lysed with saponin indicating the protease's short 34 aa N-terminal region upstream of its TM domain was projecting into the PV. The fact that the FP2a reporter was more strongly degraded in the absence of WR indicates that PTEX probably only extracts the reporter as far as the PV and not beyond (Fig 8). If PTEX could capture FP2a reporters and deliver them to the cytostome before translocating them into the cytostome lumen for uptake into vesicles, PTEX would be expected to concentrate at the cytostome, which might appear as one to a few distinct puncta at the parasite periphery (36). We observed these concentrated puncta for FP2a (S2D Fig) but we never observed a particular concentration of EXP2 overlapping with the cytostomal puncta. Instead, a continuous

565 circle or "necklace of beads" surrounding the parasite was observed as previously
566 reported, sometimes with 1-3 PVM loop extensions in older parasites (4-6, 8, 13, 53,
567 59, 74). This likely indicates that PTEX does not directly deposit Hb proteases into
568 the cytostome, however this should be more extensively investigated with markers for
569 both the cytostome (Kelch 13) and PTEX (75).
570
571 Following uptake into the PV the Hb proteases possibly employ signals within their
572 N-terminal pro-sequences to specify cytostome trafficking. This signal is likely
573 present between aa 84 to 105 of FP2a, given that truncation studies on FP2a show that
574 reporter cargoes with <84 aa of the FP2a N-terminus accumulate at the PPM but 95 aa
575 and 105 aa show partial and complete trafficking to the food vacuole, respectively
576 (35). We also found that the length of the FP2a reporter appears to be important for
577 efficient trafficking to food vacuole as the 190 aa FP2a reporter trafficked more
578 efficiently than the 120 aa reporter which could contribute to more efficient PPM
579 extraction.
580
581 In conclusion, we propose a new model for Hb protease trafficking involving PTEX
582 where the early acting FP2a, PM II and possibly other Hb proteases of these families
583 are extracted by the PTEX complex from the PPM and into the PV space. The Hb
584 proteases do not appear to be subsequently translocated across the PVM and beyond
585 into the iRBC since the 120 aa FP2a reporter was not detected in the iRBC or within
586 cargo-associated PVM loops (Fig 8). Furthermore, our FP2a reporter did not degrade
587 in the presence of EQT and proteinase K as the exported GBP130 protein did. We
588 therefore propose that HSP101 could bind to the short 34 aa N-terminal section of
589 FP2a that precedes the TM domain and projects into the PV. The HSP101/FP2a

590 complex could then dock with the rest of PTEX, which may activate HSP101 activity
591 to extract the FP2a reporter into the PV. Alternatively, the intact PTEX complex
592 could directly bind the N-terminal region of FP2a reporter and extract the protease
593 into the PV. The pro-domain of the Hb proteases could then help chaperone the
594 proteases to the lumen of the cytostome via an unknown process, where the
595 proteolytic domains could then face the interior of the Hb containing vesicles that bud
596 off the cytostome (Fig 8). Thereby, PTEX would act as a facilitator of the correct
597 orientation of the Hb proteases for their entry into the cytostome. Although our study
598 has not resolved the complete mechanism of protease transfer into the Hb containing
599 cytostomal vesicles, it could serve as a future starting point to better understand this
600 important process.
601

602 ## Material and Methods

603 ### Cloning

604 The *fp2a* gene was appended with a single HA-tag followed by a *glmS* before the 3'
605 stop codon using CRISPR/Cas9. The construct was designed using a multi-step PCR
606 where sections were amplified from 3D7 genomic DNA and sewn together with the
607 tagging sequence as shown in supplementary data (S2A Fig). The PM II-mScarlet was
608 designed the same way (S7A Fig). Flanks were then ligated into a pBSK bluescript
609 plasmid (Stratagene) and 50 µg of DNA was co-transfected into 3D7 WT (FP2a) or
610 PTEX150-HA*glmS* (PM II-mScarlet) parasites with 50 µg of a Cas9 expressing
611 plasmid (pCas9) under the U6 promoter, containing relevant guide RNA and the
612 human dihydrofolate reductase (hDHFR) cassette (76). The mutated version of the
613 Cas9 plasmid (mpCas9) was prepared for PM II-mScarlet, where the hDHFR was
614 exchanged for a Blasticidin S Deaminase (BSD) drug selection marker since the

615 PTEX150-HA*glmS* line was already WR-resistant. The BSD coding sequence from
616 pEF-Hyp1-Nluc-DH-APEX (59) was amplified in two overlapping fragments so that
617 an internal *BbsI* site could be synonymously mutated to prevent unwanted cleavage
618 prior to insertion of the guide RNA. The first BSD fragment was amplified with
619 BSD_NcoF and BbsI_MutR and the second BSD fragment was amplified with
620 BbsI_MutF and BSD_SacIIR under standard conditions. PCR fragments were then
621 sewn together with BbsI_MutF and BSD_SacIIR and the full-size BSD coding
622 sequence was excised with *NcoI* and *SacII* and ligated into similarly digested pCas9.
623 DNA primers for guide RNAs were chosen according to the list provided by (77) and
624 annealed together prior to ligation into the Cas9 plasmids, which were pre-cut with
625 *BbsI*. The pCas9 was selected for by WR (Jacobs Pharmaceutical) or mpCas9 with
626 Blasticidin S (Life technologies) for 7 days and genomic DNA extracted when
627 parasites came up to confirm correct tagging by PCR. All primers and DNA
628 sequences are listed in S2 Table.
629
630 The previously published plasmid pEF-Hyp1-Nluc-DH (53) was used to generate the
631 three different FP2a constructs, pFP2a 120/FP2a 190/ FP2a NT-Nluc-DH-FL. The
632 Hyp1 region of the reporter was removed by excision with *XhoI* and *NcoI* and
633 replaced with the relevant FP2a sequence. FP2a 120 aa and 190 aa contained the first
634 120/190 aa from the FP2a gene. To generate the FP2a NT, a forward primer was
635 designed after the TM (57 aa of the FP2a sequence) and coupled with the reverse
636 primer created for the 190 aa construct giving a ~120 aa sequence. Plasmids were
637 transfected into the HSP101-HA*glmS* parasite line and expressed episomally under
638 Blasticidin S selection. Primers are listed in S2 Table.
639

640 **Parasite culturing**

641 Continuous culture of *P. falciparum* was maintained at 4% haematocrit in human
642 RBCs in AlbumaxII media (RPMI-1640, 25 mM HEPES (Gibco), 367 µM
643 hypoxanthine (Sigma-Aldrich), 31.25 µg/mL Gentamicin (Gibco), 0.5% AlbumaxII
644 (Gibco) and 25 mM $NaHCO_3$ (AnalR)) and kept at 37 °C in gas chambers (1% O_2,
645 5% CO_2 and 96% N_2). Method adapted from Trager and Jensen (78).

646

647 **Immunofluorescence assays**

648 For WR trapping experiments, parasite culture was treated with 100 µg/mL heparin
649 (Sigma-Aldrich) to prevent invasion (79) and late schizont stages purified using a
650 67% percoll (Cytiva, diluted in PBS/RPMI) gradient. Heparin was then washed off
651 and parasites allowed to invade for 4 h. Ring stage parasites were then treated ± 10
652 nM WR. For BFA assays, parasites were synchronised in 5% sorbitol (Sigma-
653 Aldrich) for 10 min at 37 °C. Late ring/early trophozoite stage parasites were then
654 treated with 18 µM BFA/DMSO or 0.001% DMSO for 5 h and then culture harvested
655 for IFA. For haemozoin crystal experiments, HSP101-HA*glmS* and PTEX150-
656 HA*glmS* parasite lines were sorbitol synchronised at ring stage and treated ± 2.5 mM
657 GlcN at trophozoite stage and harvested the next cell cycle at late ring stage/early
658 trophozoite stage for IFA.

659

660 For all assays, parasite culture was diluted in phosphate buffered saline (PBS) and
661 mounted on Poly-L-Lysine (Sigma-Aldrich) treated coverslips (Menzel), fixed in 4%
662 paraformaldehyde/ 0.0075% glutaraldehyde in PBS for 20 min and permeabilised in
663 0.1% TX-100 (Sigma-Aldrich) with 0.1 M glycine in PBS for 15 min as previously
664 described (80, 81). Samples were blocked for 1 h in 3% bovine serum albumin

(Sigma-Aldrich) and subsequently incubated in primary antibodies (overnight) and secondary antibodies (1 h) with 3x 0.02% TX-100/PBS washes in-between. Coverslips were mounted on slides containing mounting media with DAPI (Vectashield) and sealed with nail polish. For the saponin lysis experiment, cells were incubated with ice-cold 0.05% saponin/ PBS on ice for 10 min, pelleted at 50 g for 3 min and washed 3x in 500 µL PBS. Cells were then fixed and probed with antibodies as described above. Images were visualised using the Zeiss Axio Observer Z1 inverted widefield microscope and processed using Image J software. List of antibodies can be found in S3 Table.

Pearson's correlation coefficients were used to determine co-localisation of Nluc and EXP2. Images were acquired with identical exposure settings and analysis completed on raw images using Fiji software with JACoP plugin. For the saponin lysis experiment, exposure settings were the same for the fluorescent channel of interest for all cells (± GlcN) for direct comparison of signal intensity using raw images. To measure signal only within the parasite, an area was manually drawn around the parasite using the EXP2 signal (PVM) for guidance. To quantify the signal, the integrated density of cells was measured using Image J software and signal corrected by subtracting the background fluorescence signal (cell integrated density – background mean * cell area). Background mean was measured for each field of view used for the analysis, where the average signal of three background areas was subtracted from the cells analysed within the same field of view. For haemozoin crystal experiments, the area was calculated as described for saponin experiments using the DIC channel for guidance and crystals counted as "present" or "absent" completed by two individual counters. All statistical analysis was completed using

GraphPad 8 Prism software using Student's t test with Welch correction. Number of cells analysed and replicates are indicated within each figure.

Live cell imaging

Heparin synchronised parasite culture was diluted in media 1:1 and evenly distributed over a glass slide and a coverslip placed on top and sealed with wax. Cells were visualised by microscopy as described for IFAs. Analysis was done using Image J where the mScarlet signal was categorised into either 'dot' inside the parasite or 'crescent/circle' at the parasite periphery by looking at the DIC channel and the Scarlet channel. Three individual counters completed categorisation of cells.

Growth assays

Sorbitol synchronised trophozoite stage parasite culture was adjusted to 1% haematocrit and 0.3% parasitemia and treated with 0, 0.15 or 1 mM GlcN and subsequently plated in 100 µL aliquots on 96-well plates in technical triplicate. Parasite culture was harvested at trophozoite stage in each cell cycle, for three consecutive cell cycles and stored at -80 °C until all time points had been collected. LDH was then measured as a proxy for parasite growth as previously described (50, 51), where 30 µL of parasite culture was resuspended with 75 µL of malstat reagent (0.083 M Tris, 185 mM lactic acid [adjusted to pH 7.5], 0.17% TX-100, 0.83 mM acetylpyridine adenine dinucleotide, 0.17 mg/mL Nitroblue tetrazolium, 0.08 mg/mL phenazine ethosulphate). Plates were incubated in the dark for 45 min and absorbance measured at 650 nm. Growth was normalised to time point zero (assay set up) and 0 mM GlcN set as 100% growth for each cycle. Statistical analysis was done using Student's t test with Welch correction in GraphPad Prism 8 for 2 biological replicates.

715

716 **Western blotting**

717 Trophozoite stage parasites were lysed in 0.09% saponin (Kodak) in PBS containing
718 protease inhibitors (PI, Roche) on ice for 10 min. For knockdown experiments and
719 FP2a reporter expression experiments, heparin synchronised (4 h invasion window)
720 trophozoite stage parasites were treated for one cell cycle (trophozoite to trophozoite)
721 with GlcN (Sigma-Aldrich) and parasite pellet extensively washed in PBS containing
722 protease inhibitor cocktail (PI, Roche) after saponin lysis. For other experiments,
723 parasites were sorbitol synchronised. Parasite pellets were diluted in 1x sample buffer
724 (6x: 0.3 M Tris (Astral Scientific, 60% v/v glycerol (Astral Scientific), 12 mM EDTA
725 (Sigma-Aldrich), 12% SDS (Sigma-Aldrich), 0.05% bromophenol blue (BioRad)),
726 sonicated 3x cycles (Bioruptor pico, 30 sec on/30 sec off) and reduced in 100 mM
727 Dithiothreitol (DTT, Sigma-Aldrich) prior to fractionation on 3-12% Bis-Tris gels
728 (Invitrogen). Proteins were transferred to nitrocellulose membranes (iBlot, 20V, 7
729 min), blocked in 1% casein/PBS (Sigma-Aldrich) for 1 h and incubated in primary
730 antibodies (S3 Table) overnight and in secondary antibodies for 1 h (Invitrogen) in the
731 dark. For chemiluminescence detection of chicken anti-FLAG and rat anti-RFP (to
732 detect mScarlet), the membrane was additionally incubated for 5 min in SuperSignal
733 substrate (Pierce). Blots were visualised and densitometry analysis performed using
734 the Odyssey LI-COR system. Graphs and statistical analysis, Student's t test with
735 Welch correction or simple linear regression, were completed using GraphPad 8
736 Prism Software. Full-length western blots in this study can be found in supplementary
737 information (S8 – S18 Figs).

738

739 **Co-immunoprecipitation assays**

Sorbitol synchronised ring stage parasites were treated ± 10 nM WR for ~16 h and subsequently harvested at trophozoite stage (~28-32-hpi) via magnet purification (LS, Militeyni). The iRBC pellet was resuspended in 20x pellet volume of 1x modified radioimmunoprecipitation (RIPA) buffer (1% TX-100, 0.1% SDS, 10 mM Tris [adjusted to pH 7.5], 150 mM NaCl) (56) containing PI. Cells were lysed via 2x cycles of freeze/thawing, pelleted at 16,000 g for 10 min at 4 °C and resultant supernatant was transferred to a new tube. Two different methods were used, either HA or IgG IP assays:

1) For HA IP assays, 250 µL of supernatant (~2.5 mg of protein) was diluted in 750 µL of lysis buffer and 50 µL of diluted supernatant transferred to a new tube and used as assay input. Diluted supernatant was incubated overnight with 50 µL of pre-washed 50/50 anti-HA agarose bead slurry (Sigma-Aldrich, diluted in lysis buffer)

2) For IgG IP assays, 200 µL of supernatant (2 mg of protein) was diluted in lysis buffer to make 1 mL total volume and 50 µL of diluted supernatant transferred to a new tube and used as assay input. The diluted supernatant was incubated with IgG overnight. The next day, IgG assay samples were incubated with 100 µL of pre-washed 50/50 Protein Sepharose A slurry (Sigma-Aldrich, diluted in lysis buffer) for 1 h. Samples for both HA and IgG assays were then passed through a Micro-Bio spin column (Bio-Rad) and eluted in 50 µL 1x sample buffer for 5 min at room temperature. Input was resuspended in 10 µL of 6X sample buffer and both input and elution were reduced (HA IP) by addition of in 100 mM DTT or kept non-reduced (IgG IPs) prior to SDS-PAGE and western blotting.

Proteinase K protection assay

Sorbitol synchronized trophozoite stage parasites (~24-hpi) were enriched via magnet purification and parasite pellet used immediately for proteinase K protection assays as previously described (82) but with a few modifications. 20 µL of the iRBC pellet was resuspended in 80 µL of PBS + PI supplemented with 1.6 µg of recombinant EQT (made in-house) and incubated for 10 min at 37 °C. Samples were centrifuged at 1,000 g for 3 min at 4 °C and supernatant transferred to a new tube and kept on ice. The pellet was subsequently washed 3x in PBS and divided equally between four tubes. Samples were pelleted and supernatant discarded. 100 µL PBS was added to tube 1, 100 µL PBS + proteinase K (20 µg) to tube 2, 100 µL 0.03% saponin in PBS + proteinase K to tube 3 and 100 µL of 0.25% v/v TX-100 in PBS + proteinase K to tube 4. All tubes were incubated on ice for 30 min. To stop the proteinase K activity and precipitate proteins, 11.1 µL of trichloroacetic acid (TCA, AnalR) was added to each tube, resuspended thoroughly and incubated on ice for 10 min. Samples were centrifuged at 16,000 g for 20 min at 4 °C. Supernatant was discarded and 500 µL of 100% ice-cold acetone (Merck) was added to the pellet and centrifuged at 16,000 g for 10 min at 4 °C. Supernatant was discarded and pellet left to air-dry. The dried pellet was resuspended in 100 µL of 1x sample buffer, and 26 µL of 4x sample buffer was added to EQT supernatant. All samples were reduced in 100 mM DTT and prepared for western blotting.

Metabolite extraction and analysis

Sorbitol synchronised parasite culture with ~10% trophozoite stage parasites (~24 hpi) were treated with 0, 0.15 or 1 mM GlcN plus heparin (100 µg/mL) to prevent parasite invasion. At late schizont stage the heparin was removed and parasite culture concentrated to 8% haematocrit and left shaking (85 RPM) at 37 °C for 4 h to allow

789 parasites to invade new RBCs. Culture was then sorbitol synchronised and parasite
790 pellet placed back into culture at 1% haematocrit at 37 °C. GlcN concentration was
791 maintained throughout all steps, except during sorbitol treatment. PTEX150-HA*glmS*
792 parasite culture was harvested at 18, 24 and 30-hpi or at a single time point 24-hpi
793 including additional 3D7 WT control. For metabolite extraction, samples were
794 prepared in three technical replicates, each replicate containing 1 mL warm media and
795 1x10^8 cells. All 12 tubes (0, 0.15, 1 mM GlcN and uRBCs) were incubated at 37 °C.
796 Technical triplicates were processed together for the following steps at 4 °C. Samples
797 were centrifuged at 12,000 g for 30 s, supernatant removed, and pellet resuspended in
798 1 mL ice-cold PBS. Samples were centrifuged as before, and final pellet was
799 resuspended in 200 µL of 80% acetonitrile (Merck, in Milli-Q water). The samples
800 were centrifuged at 18,000 g for 5 min, supernatant transferred to fresh tubes and
801 stored at -80 °C until processed by mass spectrometry as previously described (83).
802
803 Polar metabolite detection was performed on an Agilent 6550 Q-TOF mass
804 spectrometer operating in negative mode. Metabolites were separated on a SeQuant
805 ZIC-pHILIC column (5 µM, 150 X 4.6 mm, Millipore) using a binary gradient with a
806 1,200 series HPLC system across a 45 min method using 20 mM ammonium
807 carbonate (pH 9) and acetonitrile, as described previously (83). The scan range was
808 25-1,200 m/z between 5 and 30 min at 0.9 spectra/s. An internal reference ion
809 solution was continually run (isocratic pump at 0.2 mL/min) throughout the
810 chromatographic separation to maintain mass accuracy. Other liquid chromatography
811 parameters were: autosampler temperature 4 °C, injection volume 5-10 µL and data
812 was collected in centroid mode with Mass Hunter Workstation software (Agilent).
813 Raw Agilent.d files were converted to mzXML with MSconvert and analysed using

814 the Maven software package (84). Following alignment, metabolite identification was
815 performed either with exact mass (<10 ppm) or retention time matching to authentic
816 standards (approximately 150 in-house metabolite standards).
817

818 ## Acknowledgements

819 We thank the Australian Red Cross for the human RBCs used in this study and
820 Jacobus Pharmaceutical for providing the WR. We thank Cat Nie for technical
821 assistance with troubleshooting of the initial metabolomics experiment, analysis and
822 sample preparation. We thank Paul R. Sanders for technical assistance during the
823 preliminary work of this project. We also thank Leann Tilley and Matthew Dixon for
824 gifting the CRT, ERC and GAPDH antibodies and the Malaria Experimental Genetics
825 2018 course for providing the pCas9 plasmid.
826

827 ## Author contributions

828 T.K.J, roles: Conceptualization, Data Curation, Formal Analysis, Investigation,
829 Methodology, Validation, Visualization, Writing – Original Draft Preparation,
830 Writing – Review & Editing. B.E., roles: Conceptualization, Investigation,
831 Methodology. S.C., roles: Formal analysis, Investigation, Methodology. M.G., roles:
832 Formal Analysis, Investigation, Methodology. S.C.C., role: Investigation. M.G.D.,
833 role: Formal Analysis. M.P.S., role: Formal Analysis. M.M., roles: Resources,
834 Funding acquisition. H.E.B., roles: Conceptualization, Data curation, Funding
835 acquisition, Methodology, Project Administration, Resources, Supervision,
836 Visualization, Writing – Review & Editing. B.S.C., roles: Conceptualization, Data
837 curation, Funding acquisition, Methodology, Project Administration, Resources,
838 Supervision, Writing – Review & Editing. P.R.G., roles: Conceptualization, Data

curation, Funding acquisition, Investigation, Methodology, Project Administration, Resources, Supervision, Writing – Review & Editing

Funding

T.K.J was supported by the University of Melbourne Research Scholarship, M.G. was supported by the Deakin University Postgraduate Research Scholarship (DUPRS) and M.G.D. was supported by the Australian Government Research Training Program Scholarship. This work was supported by the Victorian Operational Infrastructure Support Program received by the Burnet Institute and by the National Health and Medical Research Council (NHMRC) grant numbers: 1092789, 1128198 and 119780521.

Conflict of interest

Authors declare no conflict of interest.

Figure legends

Fig 1. Conditional knockdown of PTEX150 perturbs the Hb digestion pathway. (A) Highly synchronous PTEX150-HA*glmS* trophozoite stage parasites were treated with 0, 0.15 or 1 mM GlcN for one cell cycle to knockdown the expression of PTEX150. The parasites were harvested at 18, 24 and 30-hpi and their metabolites were extracted and fractionated for identification by mass spectrometry. The fold change for 0.15 and 1 mM GlcN compared to untreated (UT) parasites is indicated. The amino acid sequences of the Hb peptides are shown on the left of the heat map. Heat map shows 1 biological replicate completed in technical triplicate. (B) Metabolites from 3D7 WT and PTEX150-HA*glmS* parasite lines were prepared as described for panel A and parasites harvested at 24-hpi. The heat map represents 1 biological replicate of 3 technical replicates, where fold change is shown for 0.15 or 1 mM GlcN compared to untreated. Fold change for both heat maps was calculated using the following formula =log2(GlcN treated/untreated).

Fig 2. Knockdown of PTEX150 and HSP101 results in build-up of full-length Hb inside the parasite.

(A) Trophozoite stage parasites were treated with 0, 0.15 or 1 mM GlcN for one cell cycle, harvested via saponin lysis at ~20-24-hpi and prepared for western blotting. Mouse anti-HA was used to probe for the target protein, rabbit anti-HSP70-1 was a loading control and rabbit anti-human Hb a marker for undigested Hb inside the parasites. Blots are representative of 3 biological replicates. (B) Protein band densitometry of 3 biological replicates was used to indicate the relative levels of Hb in the GlcN-induced knockdown parasites normalised to untreated parasites. 3D7 WT was used as negative control and FP2a-HA*glmS* as a positive control for Hb build-up. The densitometry for Hb was done on the monomer (indicated with an arrow in panel A). The densitometry was adjusted to the loading control and normalised to untreated to visualise changes when treated with GlcN. Error bars= SD. "%" refers to % build-up of Hb compared to untreated and "exp." refers to protein expression of the knockdown protein following GlcN treatment. Statistical analysis was completed for 1 mM GlcN comparing 3D7 WT to PTEX150, HSP101 and FP2a-HA*glmS* lines using Student's t test with Welch correction. Only FP2a showed significant increase in Hb levels compared to WT, where * P=0.0255. However, both PTEX150 and HSP101 knockdown showed trend towards Hb build-up inside the parasite when knocked down. (C) Highly synchronous PTEX150-HA*glmS* parasites were treated ± 1 mM GlcN for one cell cycle and 20-24 hpi trophozoites were lysed in saponin and prepared for IFA. Panels show representative figures from 1 biological replicate. DAPI (4',6-diamidino-2-phenylindole) was used to stain the nucleus. DIC=differential interference contrast. Scale bars= 5µm. (D) For cells from IFA experiments in panel C the integrated density (mean intensity*area) of the parasite, denoted by the boundary of EXP2 signal, was measured in the Hb channel. Statistical analyses were completed using Student's t test with Welch correction, where the number of cells analysed is indicated on the right-hand side. A significant increase in Hb integrated density was observed when parasites were treated with 1 mM GlcN compared to 0 mM GlcN, where (***) indicates P=0.0001 and error bars=SD. (E) Cells analysed in panel D were of similar size where Student's t test with Welch correction showed that there was no significant difference between treatments. Middle line represents mean and error bars=SD.

Fig 3. FP2a trappable reporters were generated to study the relationship of FP2a with PTEX.

(A) Three FP2a reporters were generated. 120 aa and 190 aa containing the first 120 aa and 190 aa of FP2a respectively. The NT reporter refers to the 190 aa reporter without the N-terminal TM domain and served as a negative control. All FP2a sequences were appended with nanoluciferase (Nluc), murine dihydrofolate reductase (DH) and a 3X FLAG (FL) epitope tag. The complete protein map for FP2a is indicated above for reference, where the reporter only contains the N-terminus sufficient for food vacuole delivery and not the C-terminus necessary for protease activity. The reporters were episomally expressed from a plasmid under the bidirectional EF1a promoter in the HSP101-HA*glmS* parental line and maintained under Blasticidin-S selection via the Blasticidin-S Deaminase (BSD) cassette. (B) Western blot analysis demonstrated that the 120 aa, 190 aa and NT FP2a reporters are expressed and migrate at the correct size indicated in panel A. Rabbit anti-Nluc was used to detect the Nluc tag and chicken anti-FLAG to detect the FL tag. Mouse anti-EXP2 was used as a loading control. (C) Immunofluorescence assays show that the 120 aa and 190 aa FP2a reporters are trafficked to the food vacuole. The NT FP2a reporter displayed diffuse labelling within the parasite as expected. Rabbit anti-Nluc

was used to detect the reporter, mouse anti-EXP2 was used as a PVM marker and haemozoin crystals in the DIC show food vacuole localisation (indicated with a white dotted line). (D) Late ring/early trophozoites were treated ± 18 µM BFA to inhibit ER to Golgi protein secretion. The 120 and 190 aa FP2a reporters were both trapped in the ER upon BFA treatment as expected and no changes were observed for the NT reporter. Rabbit anti-ERC was used as an ER marker and mouse anti-HA to label for HSP101, which also traps in the ER upon BFA treatment (53). DAPI was used to stain the nucleus. Scale bars = 5 µm.

Fig 4. The FP2a 120 aa reporter shows significantly more association with EXP2 upon WR trapping.

(A) Parasites expressing the 120 aa, 190 aa and NT FP2a reporters were synchronised and treated ± 10 nM WR at ring stage to prevent unfolding of the reporters to see if they would become trapped at the parasite periphery with PTEX. When treated with WR, more 120 aa reporter was observed at the PPM/PVM indicating its trafficking was affected. No substantial difference was observed for 190 aa or NT reporters. Shown are representative images for 3 (120 aa) and 2 (190 aa and NT) biological replicates. Rabbit anti-EXP2 was used as a PVM marker, rabbit anti-Nluc to detect the reporters and DAPI to stain the nucleus. Scale bars= 5 µm. Arrows point to PVM loops. (B) Pearson's coefficient was used to measure the co-localisation of the FP2a reporters (Nluc) and EXP2. There was significantly more co-localisation of 120 aa with EXP2 when treated with WR as determined by student's t test with Welch correction but no significant difference was observed for the 190 aa or NT reporters. (****) Indicates P <0.0001, n= cells analysed (pooled from 3 (120 aa) or 2 (190 aa and NT) biological replicates), middle line on the graph represents mean and error bars=SD. Each dot on the graph represents a cell analysed.

Fig 5. Both the 120 aa and the 190 aa FP2a reporters interact with HSP101 and this interaction is weaker when reporters are inhibited from unfolding via addition of WR.

(A) Ring stage HSP101-HA*glmS* parasites episomally expressing Hyp1, NT, 120 aa, or 190 aa reporters were treated ± 10 nM WR and harvested at trophozoite stage (~28-32 hpi). Anti-HA IgG beads were used to IP HSP101 and its interacting proteins. Input shows 1% protein lysate used for the assay, and elution refers to protein bound to the HA beads/HSP101-HA*glmS* indicating their interaction with HSP101. Hyp1 was used as positive control and NT as a negative control. Mouse anti-HA was used to probe for HSP101, chicken anti-FLAG for the reporter, rabbit anti-741 for PTEX150 and mouse anti-EXP2 for EXP2. Blot is representative of 3 biological replicates. The asterisks indicate stronger signal when comparing the ± WR treatment for respective reporter as determined by densitometry of all biological replicates. (B) The interaction of reporters with HSP101 was graphed, where FLAG elution was adjusted to input. Each dot represents 1 biological replicate. (C) The interaction of reporters with HSP101, where the fold difference of the FLAG elution/input was adjusted to untreated (-WR). Error bars= SD from 3 biological replicates.

Fig 6. Proteinase K protection assay shows that FP2a needs to be unfolded before crossing the PPM with its N-terminus first.

(A) Ring stage parasites were treated ± 10 nM WR to inhibit the 120 aa FP2a reporter from unfolding. Trophozoite stage parasites were magnet purified and used

for proteinase K (PK) protection assays. EQT was used to permeabilise the iRBC membrane, saponin (SAP) to lyse the PVM, and TX-100 to lyse all membranes. A 3.8 kDa shift was observed in the reporter size when the PV was lysed and treated with PK (lanes 4 and 9), which matches the predicted size of the 34 aa (4 kDa) N-terminus preceding TM domain (measured in Odyssey LICOR). FP2a reporter appears to be more protected against PK degradation when treated with WR vs. non-treated, indicating trapping at the PPM not PVM. Chicken anti-FLAG was used to probe for the FP2a reporter, GBP130 is a soluble exported protein marker, SERA5 is a PV marker and GAPDH is a parasite cytoplasm marker. Blot is representative of 3 biological replicates, which showed a similar trend, SN= supernatant, P= pellet. (B) The fold difference for protection of the FP2a reporter (FLAG) was measured by densitometry, where the FLAG signal was adjusted to GAPDH and the fold difference measured by adjusting the EQT + PK and SAP + PK signal to EQT + PBS. The fold difference (X) compared with untreated is indicated with a red dotted line on the graph. Error bars = SD from 3 biological replicates. (C) A suggested model derived from the PK assay results. When parasites were not treated with WR more reporter cargo was degraded indicating that when inhibited from unfolding the reporter was trapped at the PPM. This likely hindered extraction into the PV potentially facilitated by HSP101 as suggested for TM exported proteins.

Fig 7. The PM II-mScarlet fusion protein in the PTEX150-HA*glmS* parental line accumulates at the parasite periphery when PTEX150 is knocked down and co-precipitates with PTEX150.

(A) Western blot was used to confirm the correct size of PM II-mScarlet, detected by rat anti-RFP (red fluorescent protein), which detects the mScarlet tag. Mouse anti-HA was used to detect the PTEX150-HA*glmS* of the parental line and rabbit anti-HSP70-1 was used as a loading control. Only the pro form of the protease was detected. (B) Live cell microscopy was used to visualise the localisation of the mScarlet (PM II) in both ring and trophozoite stage parasites, where the tag was observed inside the parasite and overlapping with the food vacuole (haemozoin crystals), which are indicated with a dotted white line. Scale bars= 5 µm. (C) PM II-mScarlet parasites were treated ± 1 mM GlcN at trophozoite stage and harvested at late ring/early trophozoite stage (~20 hpi) for live cell microscopy. The mScarlet signal was subsequently categorised as either 'dot' or 'crescent/circle' around the parasite periphery. Panel shows representative images for each category, the experiment was completed in 3 biological replicates. Scale bars=5µm. (D) Graphs show the percentage of parasites with dots vs. crescent/circular labelling from the experiment in panel C. Statistical analysis was completed using Student's t test with Welch correction. n = total number of cells counted per condition with 3 biological replicates combined. Error bars= SD for 3 individuals counting. (**) Indicates P= 0.0048. (E) Anti-HA IgG beads were used to IP PTEX150 and its interacting proteins. EXP2 and HSP101 were used as positive control for interaction, GAPDH as a negative control and 3D7 WT as a negative control for non-specific interaction with beads. Blot is representative of 2 biological replicates.

Fig 8. Model depicting newly identified steps in the FP2a trafficking pathway to the food vacuole.

By integrating the data from this study, we propose a new model for the trafficking of FP2a, and potentially other Hb proteases, to the food vacuole. (A) The FP2a protein enters the secretory pathway and travels from the ER to the PV, (B) where the protein

is deposited in the PPM via its TM domain (pink), in an N- to C-terminal direction. (C) HSP101 could help extract FP2a from the PPM and into the PV as proposed for TM exported proteins and then interact with the rest of PTEX, or (D) all the PTEX core components could participate in FP2a extraction from the PPM. FP2a is then escorted to the cytostome, which likely involves additional sorting in the PV by an unknown mechanism. (E) The proteolytic domain (purple) of FP2a is likely placed with the C-terminus inside the cytostome for easy access to the Hb, which is taken up via the cytostome formed by invagination of the PVM and PPM. (F) FP2a is then transported to the food vacuole (FV) together with Hb. (G) Inside the FV the Hb is digested into smaller peptides, releasing haem, which is sequestered into haemozoin crystals (Hz). (H) Reduced PTEX expression results in accumulation of Hb proteases (as shown with PM II-mScarlet) at the parasite periphery. (I) This would subsequently lead to accumulation of full-length Hb inside the FV and reduced levels of haemozoin crystal formation. Figure is partially based on Hb trafficking models provided by (32, 38). A Red cross is drawn over FP2a incorporation into the PVM by PTEX, as this is likely not possible since PTEX does not have lateral gate to facilitate this.

Supporting information

S1 Fig. Metabolite heat maps.
(A) Heat map corresponding to S1 Table for PTEX150-HA*glmS* metabolomics time course (18, 24, 30-hpi) experiment. (B) Heat map corresponding to S1 Table for 3D7 and PTEX150-HA*glmS* metabolomics experiment. Numbers represent metabolites listed in S1 Table, where Hb peptides have been highlighted in bold. Fold change for both heat maps was calculated using the following formula =log2(GlcN treated/untreated).

S2 Fig. Generation and characterisation of the FP2a-HA*glmS* parasite line.
(A) CRISPR-Cas9 was used to append the *fp2a* gene with a HA tag and a *glmS* riboswitch. (B) PCR was used to confirm the correct integration of the tag to the target gene, where 3D7 WT was used as a negative control for integration. The position of PCR primers used to confirm integration are shown in panel A, where FInt, is the forward PCR integration primer. F, forward primer. glmS_R, reverse primer. (C) Correct size and level of FP2a knockdown was confirmed using western blotting. >90% of FP2a was knocked down after one cell cycle of GlcN treatment. P stands for pro FP2a and M stands for mature FP2a. The HA-tag adds approximately 3 kDa to the target protein. The mark on the right-hand side of the blot is an artefact. Mouse anti-HA detects FP2a-HA*glmS* and rabbit anti-HSP70-1 was used as a loading control. Blot is representative of 3 biological replicates. (D) Immunofluorescence assays where mouse anti-HA detects target protein and rabbit anti-EXP2 was used as a PVM marker. The images indicate that FP2a displays diffused localisation in the parasite cytoplasm, sometimes with a concentrated puncta at the parasite periphery, likely representing the cytostome (white arrows). The HA antibody signal against FP2a-HA*glmS* partly overlaps with rabbit anti-CRT which labels the food vacuole membranes. Food vacuole lumen, indicated by the dark haemozoin crystals in the DIC images, are not well labelled for FP2a-HA*glmS* likely due to the HA epitope tag being proteolytically degraded in the food vacuole. Scale bars= 5 μm. (E) Multi-cycle LDH growth assays were performed over 3 consecutive cell cycles. No significant growth defect was observed for FP2a or 3D7 WT when treated with different concentrations of GlcN. T = number of cycles. Statistics were completed using

Student's t test with Welch correction. Graphs show 2 biological replicates completed in technical triplicate. Error bars= SD. Data for each parasite line was normalised to 0 GlcN treatment for each time point.

S3 Fig. Knockdown of PTEX150 and HSP101 results in build-up of full-length Hb inside the parasite and reduced haemozoin crystal formation.
(A) Simple linear regression analysis was performed on protein expression and Hb build-up from western blots presented in Fig 2B for PTEX150-HA*glmS*, HSP101-HA*glmS* and FP2a-HA*glmS*. All parasite lines showed significant regression slope, where P values are shown in each graph along with R^2. The 6 blue dots on the graphs represent 3 biological replicates for 0.15 and 1 mM GlcN for protein expression (x-axis) plotted against the mean for 3 biological replicates for Hb build-up (y-axis). (B) Both PTEX150-HA*glmS* and HSP101-HA*glmS* trophozoite stage parasites were treated ± 2.5 mM GlcN for one cell cycle and harvested for IFA. Haemozoin crystals in the DIC channel were counted (present or absent). Images are representative of 3 (PTEX150) or 2 (HSP101) biological replicates. (C) Both PTEX150 and HSP101 knockdown experiments shown in panel B resulted in significantly less crystal formation compared to untreated cells when using Student's t test with Welch correction. (*) Indicates P= 0.0247 (PTEX150) and P=0.0277 (HSP101). Error bars = SD from 2 individuals counting. (D) Area of the parasites analysed in panel C (completed as described in Fig 2E) showed significant difference in size for GlcN treated PTEX150 parasites compared with untreated indicating parasite growth was affected but no significant difference was observed for HSP101 knockdown. Middle line represents mean and error bars=SD. (****) Indicates P=<0.0001. Each dot on the graph represents one cell analysed.

S4 Fig. Western blot time course indicates that the 120 and 190 aa FP2a reporters are expressed similarly from 24-40-hpi while the NT reporter is degraded as the parasite matures.
Synchronous (4 h invasion window) parasite cultures for the three FP2a reporter lines were divided in four and harvested via saponin lysis at four sequential time points: 24-28 hpi, 28-32 hpi, 32-36 hpi and 36-40 hpi. Chicken anti-FLAG and rabbit anti-Nluc were used to visualise the FP2a reporters, mouse anti-HA to visualise the HSP101-HA*glmS* (parental line) and rabbit anti-HSP70-1 was used as a loading control. The expected size of each reporter is indicated with (*), where the cleavage of Nluc from the 120 and 190 aa reporters was observed in each time point (lanes 2, 3, 5, 6, 8, 9, 11 and 12), likely due to cleavage upon entry into the food vacuole. This cleavage of Nluc was not observed for the NT reporter (lanes 1, 4, 7 and 10), which does not enter the food vacuole. The NT reporter was also degraded more, and the expression of the full-length reporter diminishes as the parasite matures (lanes 1 and 4 vs. lanes 7 and 10), whilst expression of the 120 and 190 aa reporters remains stable across each time point. These data indicate that the optimal time point to study these three reporters was in the range of 24-32 hpi, as indicated in bold. This blot represents 2 biological replicates.

S5 Fig. The 120 aa and the 190 aa FP2a reporters interact with PTEX150 and EXP2.
Immunoprecipitation assays with parasites treated with ± 10 nM WR were completed on the four reporter lines using Protein Sepharose A where (A) PTEX150 or (B) EXP2 protein specific antibodies were incubated with parasite lysate to Co-IP

interacting proteins. Both 120 aa (line 13) and 190 aa (line 15) showed stronger association with (A) PTEX150 and (B) EXP2 in –WR treatment as determined by densitometry (S6 Fig). The Hyp1 reporter showed reverse association to FP2a reporters and NT showed some background signal in both conditions. (A) PTEX150 and (B) EXP2 both co-precipitated with other PTEX components (lanes 9 – 16). Chicken anti-FLAG was used to probe for the reporter, mouse anti-HA for HSP101 and rabbit 741 for PTEX150. Both (A) and (B) blots represent 3 biological replicates. The asterisks indicate stronger signal when comparing the ± WR treatment for respective reporter measured by densitometry of 3 biological replicates.

S6 Fig. Densitometry measurements for PTEX150 and EXP2 IPs.
(A) The interaction of reporters with PTEX150 (r942) and EXP2 (r1167) presented in S5 Fig A was graphed, where FLAG elution was adjusted to input. Each dot represents 1 biological replicate. (B) The interaction of reporters with PTEX150 (r942) and EXP2 (r1167), where the fold difference of the FLAG elution/input was adjusted to untreated (-WR). Error bars= SD from 3 biological replicates.

S7 Fig. Establishment of PM II mScarlet in a PTEX150-HA*glmS* background.
(A) The *pm ii* gene was C-terminally tagged with mScarlet as described for FP2a in S2 Fig A and introduced into a PTEX150-HA*glmS* background. (B) Correct integration of mScarlet to PM II was confirmed via PCR, where genotyping primers are displayed in panel A.

S8 – S18 Figs. Full-length western blots presented in this study.

References

1. W.H.O. World Malaria Report 2021. Geneva: World Health Organisation; 2021.
2. Milner DA, Jr. Malaria Pathogenesis. Cold Spring Harb Perspect Med. 2018;8(1):a025569.
3. Marti M, Spielmann T. Protein export in malaria parasites: many membranes to cross. Curr Opin Microbiol. 2013;16(4):445-51.
4. de Koning-Ward TF, Gilson PR, Boddey JA, Rug M, Smith BJ, Papenfuss AT, et al. A newly discovered protein export machine in malaria parasites. Nature. 2009;459(7249):945-9.
5. Beck JR, Muralidharan V, Oksman A, Goldberg DE. PTEX component HSP101 mediates export of diverse malaria effectors into host erythrocytes. Nature. 2014;511(7511):592-5.
6. Elsworth B, Matthews K, Nie CQ, Kalanon M, Charnaud SC, Sanders PR, et al. PTEX is an essential nexus for protein export in malaria parasites. Nature. 2014;511(7511):587-91.
7. Charnaud SC, Kumarasingha R, Bullen HE, Crabb BS, Gilson PR. Knockdown of the translocon protein EXP2 in *Plasmodium falciparum* reduces growth and protein export. PLoS One. 2018;13(11):e0204785.
8. Bullen HE, Charnaud SC, Kalanon M, Riglar DT, Dekiwadia C, Kangwanrangsan N, et al. Biosynthesis, localization, and macromolecular

arrangement of the *Plasmodium falciparum* translocon of exported proteins (PTEX). J Biol Chem. 2012;287(11):7871-84.

9. Ho CM, Beck JR, Lai M, Cui Y, Goldberg DE, Egea PF, et al. Malaria parasite translocon structure and mechanism of effector export. Nature. 2018;561(7721):70-5.

10. Matthews KM, Kalanon M, de Koning-Ward TF. Uncoupling the threading and unfoldase actions of *Plasmodium* HSP101 reveals differences in export between soluble and insoluble proteins. mBio. 2019;10(3).

11. Matthews K, Kalanon M, Chisholm SA, Sturm A, Goodman CD, Dixon MW, et al. The *Plasmodium* translocon of exported proteins (PTEX) component thioredoxin-2 is important for maintaining normal blood-stage growth. Mol Microbiol. 2013;89(6):1167-86.

12. Matz JM, Matuschewski K, Kooij TW. Two putative protein export regulators promote *Plasmodium* blood stage development *in vivo*. Mol Biochem Parasitol. 2013;191(1):44-52.

13. Garten M, Nasamu AS, Niles JC, Zimmerberg J, Goldberg DE, Beck JR. EXP2 is a nutrient-permeable channel in the vacuolar membrane of *Plasmodium* and is essential for protein export via PTEX. Nat Microbiol. 2018;3(10):1090-8.

14. van Ooij C, Tamez P, Bhattacharjee S, Hiller NL, Harrison T, Liolios K, et al. The malaria secretome: from algorithms to essential function in blood stage infection. PLoS Pathog. 2008;4(6):e1000084.

15. Sargeant TJ, Marti M, Caler E, Carlton JM, Simpson K, Speed TP, et al. Lineage-specific expansion of proteins exported to erythrocytes in malaria parasites. Genome Biol. 2006;7(2):R12.

16. Boddey JA, Carvalho TG, Hodder AN, Sargeant TJ, Sleebs BE, Marapana D, et al. Role of plasmepsin V in export of diverse protein families from the *Plasmodium falciparum* exportome. Traffic. 2013;14(5):532-50.

17. Hiller NL, Bhattacharjee S, van Ooij C, Liolios K, Harrison T, Lopez-Estrano C, et al. A host-targeting signal in virulence proteins reveals a secretome in malarial infection. Science. 2004;306(5703):1934-7.

18. Marti M, Good RT, Rug M, Knuepfer E, Cowman AF. Targeting malaria virulence and remodeling proteins to the host erythrocyte. Science. 2004;306(5703):1930-3.

19. Heiber A, Kruse F, Pick C, Gruring C, Flemming S, Oberli A, et al. Identification of new PNEPs indicates a substantial non-PEXEL exportome and underpins common features in *Plasmodium falciparum* protein export. PLoS Pathog. 2013;9(8):e1003546.

20. Maier AG, Rug M, O'Neill MT, Brown M, Chakravorty S, Szestak T, et al. Exported proteins required for virulence and rigidity of *Plasmodium falciparum*-infected human erythrocytes. Cell. 2008;134(1):48-61.

21. Jonsdottir TK, Gabriela M, Crabb BS, T FdK-W, Gilson PR. Defining the essential exportome of the malaria parasite. Trends Parasitol. 2021;37(7):664-75.

22. Nguitragool W, Bokhari AA, Pillai AD, Rayavara K, Sharma P, Turpin B, et al. Malaria parasite *clag3* genes determine channel-mediated nutrient uptake by infected red blood cells. Cell. 2011;145(5):665-77.

23. Counihan NA, Chisholm SA, Bullen HE, Srivastava A, Sanders PR, Jonsdottir TK, et al. *Plasmodium falciparum* parasites deploy RhopH2 into the host erythrocyte to obtain nutrients, grow and replicate. Elife. 2017;6:e23217.

24. Ito D, Schureck MA, Desai SA. An essential dual-function complex mediates erythrocyte invasion and channel-mediated nutrient uptake in malaria parasites. Elife. 2017;6:e23485.
25. Sherling ES, Knuepfer E, Brzostowski JA, Miller LH, Blackman MJ, van Ooij C. The *Plasmodium falciparum* rhoptry protein RhopH3 plays essential roles in host cell invasion and nutrient uptake. Elife. 2017;6:e23239.
26. Ahmad M, Manzella-Lapeira J, Saggu G, Ito D, Brzostowski JA, Desai SA. Live-cell FRET reveals that malaria nutrient channel proteins CLAG3 and RhopH2 remain associated throughout their tortuous trafficking. mBio. 2020;11(5):e01354-20.
27. Pasternak M, Verhoef JMJ, Wong W, Triglia T, Mlodzianoski MJ, Geoghegan N, et al. RhopH2 and RhopH3 export enables assembly of the RhopH complex on *P. falciparum*-infected erythrocyte membranes. Commun Biol. 2022;5(1):333.
28. Maier AG, Cooke BM, Cowman AF, Tilley L. Malaria parasite proteins that remodel the host erythrocyte. Nat Rev Microbiol. 2009;7(5):341-54.
29. Gomes PS, Bhardwaj J, Rivera-Correa J, Freire-De-Lima CG, Morrot A. Immune escape strategies of malaria parasites. Front Microbiol. 2016;7:1617.
30. de Koning-Ward TF, Dixon MW, Tilley L, Gilson PR. *Plasmodium* species: master renovators of their host cells. Nat Rev Microbiol. 2016;14(8):494-507.
31. Prommana P, Uthaipibull C, Wongsombat C, Kamchonwongpaisan S, Yuthavong Y, Knuepfer E, et al. Inducible knockdown of *Plasmodium* gene expression using the *glmS* ribozyme. PLoS One. 2013;8(8):e73783.
32. Milani KJ, Schneider TG, Taraschi TF. Defining the morphology and mechanism of the hemoglobin transport pathway in *Plasmodium falciparum*-infected erythrocytes. Eukaryot Cell. 2015;14(4):415-26.
33. Egan TJ, Combrinck JM, Egan J, Hearne GR, Marques HM, Ntenteni S, et al. Fate of haem iron in the malaria parasite *Plasmodium falciparum*. Biochem J. 2002;365(Pt 2):343-7.
34. Dasaradhi PV, Korde R, Thompson JK, Tanwar C, Nag TC, Chauhan VS, et al. Food vacuole targeting and trafficking of falcipain-2, an important cysteine protease of human malaria parasite *Plasmodium falciparum*. Mol Biochem Parasitol. 2007;156(1):12-23.
35. Subramanian S, Sijwali PS, Rosenthal PJ. Falcipain cysteine proteases require bipartite motifs for trafficking to the *Plasmodium falciparum* food vacuole. J Biol Chem. 2007;282(34):24961-9.
36. Klemba M, Beatty W, Gluzman I, Goldberg DE. Trafficking of plasmepsin II to the food vacuole of the malaria parasite *Plasmodium falciparum*. J Cell Biol. 2004;164(1):47-56.
37. Lazarus MD, Schneider TG, Taraschi TF. A new model for hemoglobin ingestion and transport by the human malaria parasite *Plasmodium falciparum*. J Cell Sci. 2008;121(11):1937-49.
38. Abu Bakar N, Klonis N, Hanssen E, Chan C, Tilley L. Digestive-vacuole genesis and endocytic processes in the early intraerythrocytic stages of *Plasmodium falciparum*. J Cell Sci. 2010;123(Pt 3):441-50.
39. Krugliak M, Zhang J, Ginsburg H. Intraerythrocytic *Plasmodium falciparum* utilizes only a fraction of the amino acids derived from the digestion of host cell cytosol for the biosynthesis of its proteins. Mol Biochem Parasitol. 2002;119(2):249-56.

40. Lew VL, Tiffert T, Ginsburg H. Excess hemoglobin digestion and the osmotic stability of *Plasmodium falciparum*-infected red blood cells. Blood. 2003;101(10):4189-94.
41. Esposito A, Tiffert T, Mauritz JM, Schlachter S, Bannister LH, Kaminski CF, et al. FRET imaging of hemoglobin concentration in *Plasmodium falciparum*-infected red cells. PLoS One. 2008;3(11):e3780.
42. Goldberg DE, Slater AF, Beavis R, Chait B, Cerami A, Henderson GB. Hemoglobin degradation in the human malaria pathogen *Plasmodium falciparum*: a catabolic pathway initiated by a specific aspartic protease. J Exp Med. 1991;173(4):961-9.
43. Dahl EL, Rosenthal PJ. Biosynthesis, localization, and processing of falcipain cysteine proteases of *Plasmodium falciparum*. Mol Biochem Parasitol. 2005;139(2):205-12.
44. Banerjee R, Liu J, Beatty W, Pelosof L, Klemba M, Goldberg DE. Four plasmepsins are active in the *Plasmodium falciparum* food vacuole, including a protease with an active-site histidine. Proc Natl Acad Sci U S A. 2002;99(2):990-5.
45. Sijwali PS, Rosenthal PJ. Gene disruption confirms a critical role for the cysteine protease falcipain-2 in hemoglobin hydrolysis by *Plasmodium falciparum*. Proc Natl Acad Sci U S A. 2004;101(13):4384-9.
46. Omara-Opyene AL, Moura PA, Sulsona CR, Bonilla JA, Yowell CA, Fujioka H, et al. Genetic disruption of the *Plasmodium falciparum* digestive vacuole plasmepsins demonstrates their functional redundancy. J Biol Chem. 2004;279(52):54088-96.
47. Shenai BR, Sijwali PS, Singh A, Rosenthal PJ. Characterization of native and recombinant falcipain-2, a principal trophozoite cysteine protease and essential hemoglobinase of *Plasmodium falciparum*. J Biol Chem. 2000;275(37):29000-10.
48. Klonis N, Tan O, Jackson K, Goldberg D, Klemba M, Tilley L. Evaluation of pH during cytostomal endocytosis and vacuolar catabolism of haemoglobin in *Plasmodium falciparum*. Biochem J. 2007;407(3):343-54.
49. Matz JM, Drepper B, Blum TB, van Genderen E, Burrell A, Martin P, et al. A lipocalin mediates unidirectional heme biomineralization in malaria parasites. Proc Natl Acad Sci U S A. 2020;117(28):16546-56.
50. Makler MT, Hinrichs DJ. Measurement of the lactate dehydrogenase activity of *Plasmodium falciparum* as an assessment of parasitemia. Am J Trop Med Hyg. 1993;48(2):205-10.
51. Persson KE, Lee CT, Marsh K, Beeson JG. Development and optimization of high-throughput methods to measure *Plasmodium falciparum*-specific growth inhibitory antibodies. J Clin Microbiol. 2006;44(5):1665-73.
52. Sijwali PS, Koo J, Singh N, Rosenthal PJ. Gene disruptions demonstrate independent roles for the four falcipain cysteine proteases of *Plasmodium falciparum*. Mol Biochem Parasitol. 2006;150(1):96-106.
53. Gabriela M, Matthews KM, Boshoven C, Kouskousis B, Jonsdottir TK, Bullen HE, et al. A revised mechanism for how *Plasmodium falciparum* recruits and exports proteins into its erythrocytic host cell. PLoS Pathog. 2022;18(2):e1009977.
54. Egan TJ. Recent advances in understanding the mechanism of hemozoin (malaria pigment) formation. J Inorg Biochem. 2008;102(5-6):1288-99.

55. Azevedo MF, Nie CQ, Elsworth B, Charnaud SC, Sanders PR, Crabb BS, et al. *Plasmodium falciparum* transfected with ultra bright NanoLuc luciferase offers high sensitivity detection for the screening of growth and cellular trafficking inhibitors. PLoS One. 2014;9(11):e112571.
56. Mesen-Ramirez P, Reinsch F, Blancke Soares A, Bergmann B, Ullrich AK, Tenzer S, et al. Stable translocation intermediates jam global protein export in *Plasmodium falciparum* parasites and link the PTEX component EXP2 with translocation activity. PLoS Pathog. 2016;12(5):e1005618.
57. Eilers M, Schatz G. Binding of a specific ligand inhibits import of a purified precursor protein into mitochondria. Nature. 1986;322(6076):228-32.
58. Gehde N, Hinrichs C, Montilla I, Charpian S, Lingelbach K, Przyborski JM. Protein unfolding is an essential requirement for transport across the parasitophorous vacuolar membrane of *Plasmodium falciparum*. Mol Microbiol. 2009;71(3):613-28.
59. Charnaud SC, Jonsdottir TK, Sanders PR, Bullen HE, Dickerman BK, Kouskousis B, et al. Spatial organization of protein export in malaria parasite blood stages. Traffic. 2018;19(8):605-23.
60. Benting J, Mattei D, Lingelbach K. Brefeldin A inhibits transport of the glycophorin-binding protein from *Plasmodium falciparum* into the host erythrocyte. Biochem J. 1994;300 (Pt 3):821-6.
61. Crary JL, Haldar K. Brefeldin A inhibits protein secretion and parasite maturation in the ring stage of *Plasmodium falciparum*. Mol Biochem Parasitol. 1992;53(1-2):185-92.
62. Bullen HE, Sanders PR, Dans MG, Jonsdottir TK, Riglar DT, Looker O, et al. The *Plasmodium falciparum* parasitophorous vacuole protein P113 interacts with the parasite protein export machinery and maintains normal vacuole architecture. Mol Microbiol. 2022;117(5):1245-62.
63. Jackson KE, Spielmann T, Hanssen E, Adisa A, Separovic F, Dixon MW, et al. Selective permeabilization of the host cell membrane of *Plasmodium falciparum*-infected red blood cells with streptolysin O and equinatoxin II. Biochem J. 2007;403(1):167-75.
64. Perkins M. Stage-dependent processing and localization of a *Plasmodium falciparum* protein of 130,000 molecular weight. Exp Parasitol. 1988;65(1):61-8.
65. Blackman MJ. Malarial proteases and host cell egress: an 'emerging' cascade. Cell Microbiol. 2008;10(10):1925-34.
66. Klemba M, Gluzman I, Goldberg DE. A *Plasmodium falciparum* dipeptidyl aminopeptidase I participates in vacuolar hemoglobin degradation. J Biol Chem. 2004;279(41):43000-7.
67. Gupta P, Pandey R, Thakur V, Parveen S, Kaur I, Panda A, et al. Heme Detoxification Protein (PfHDP) is essential for the hemoglobin uptake and metabolism in *Plasmodium falciparum*. FASEB BioAdvances. 2022;00:1-13.
68. Mesen-Ramirez P, Bergmann B, Tran TT, Garten M, Stacker J, Naranjo-Prado I, et al. EXP1 is critical for nutrient uptake across the parasitophorous vacuole membrane of malaria parasites. PLoS Biol. 2019;17(9):e3000473.
69. Drew ME, Banerjee R, Uffman EW, Gilbertson S, Rosenthal PJ, Goldberg DE. *Plasmodium* food vacuole plasmepsins are activated by falcipains. J Biol Chem. 2008;283(19):12870-6.

70. Gruring C, Heiber A, Kruse F, Flemming S, Franci G, Colombo SF, et al. Uncovering common principles in protein export of malaria parasites. Cell Host Microbe. 2012;12(5):717-29.
71. Matthews KM, Pitman EL, de Koning-Ward TF. Illuminating how malaria parasites export proteins into host erythrocytes. Cell Microbiol. 2019;21(4):e13009.
72. Egea PF, Stroud RM. Lateral opening of a translocon upon entry of protein suggests the mechanism of insertion into membranes. Proc Natl Acad Sci U S A. 2010;107(40):17182-7.
73. Schureck MA, Darling JE, Merk A, Shao J, Daggupati G, Srinivasan P, et al. Malaria parasites use a soluble RhopH complex for erythrocyte invasion and an integral form for nutrient uptake. Elife. 2021;10:e65282.
74. Riglar DT, Rogers KL, Hanssen E, Turnbull L, Bullen HE, Charnaud SC, et al. Spatial association with PTEX complexes defines regions for effector export into *Plasmodium falciparum*-infected erythrocytes. Nat Commun. 2013;4:1415.
75. Birnbaum J, Scharf S, Schmidt S, Jonscher E, Hoeijmakers WAM, Flemming S, et al. A Kelch13-defined endocytosis pathway mediates artemisinin resistance in malaria parasites. Science. 2020;367(6473):51-9.
76. Adjalley S, Lee MCS. CRISPR/Cas9 Editing of the *Plasmodium falciparum* Genome. Methods Mol Biol. 2022;2470:221-39.
77. Ribeiro JM, Garriga M, Potchen N, Crater AK, Gupta A, Ito D, et al. Guide RNA selection for CRISPR-Cas9 transfections in *Plasmodium falciparum*. Int J Parasitol. 2018;48(11):825-32.
78. Trager W, Jensen JB. Human malaria parasites in continuous culture. Science. 1976;193(4254):673-5.
79. Boyle MJ, Richards JS, Gilson PR, Chai W, Beeson JG. Interactions with heparin-like molecules during erythrocyte invasion by *Plasmodium falciparum* merozoites. Blood. 2010;115(22):4559-68.
80. Jonsdottir TK, Counihan NA, Modak JK, Kouskousis B, Sanders PR, Gabriela M, et al. Characterisation of complexes formed by parasite proteins exported into the host cell compartment of *Plasmodium falciparum* infected red blood cells. Cellular Microbiology. 2021;23(8):e13332.
81. Tonkin CJ, van Dooren GG, Spurck TP, Struck NS, Good RT, Handman E, et al. Localization of organellar proteins in *Plasmodium falciparum* using a novel set of transfection vectors and a new immunofluorescence fixation method. Mol Biochem Parasitol. 2004;137(1):13-21.
82. Sanders PR, Dickerman BK, Charnaud SC, Ramsland PA, Crabb BS, Gilson PR. The N-terminus of EXP2 forms the membrane-associated pore of the protein exporting translocon PTEX in *Plasmodium falciparum*. J Biochem. 2019;165(3):239-48.
83. Cobbold SA, Chua HH, Nijagal B, Creek DJ, Ralph SA, McConville MJ. Metabolic dysregulation induced in *Plasmodium falciparum* by dihydroartemisinin and other front-line antimalarial drugs. J Infect Dis. 2016;213(2):276-86.
84. Clasquin MF, Melamud E, Rabinowitz JD. LC-MS data processing with MAVEN: a metabolomic analysis and visualization engine. Curr Protoc Bioinformatics. 2012;Chapter 14:Unit14 1.

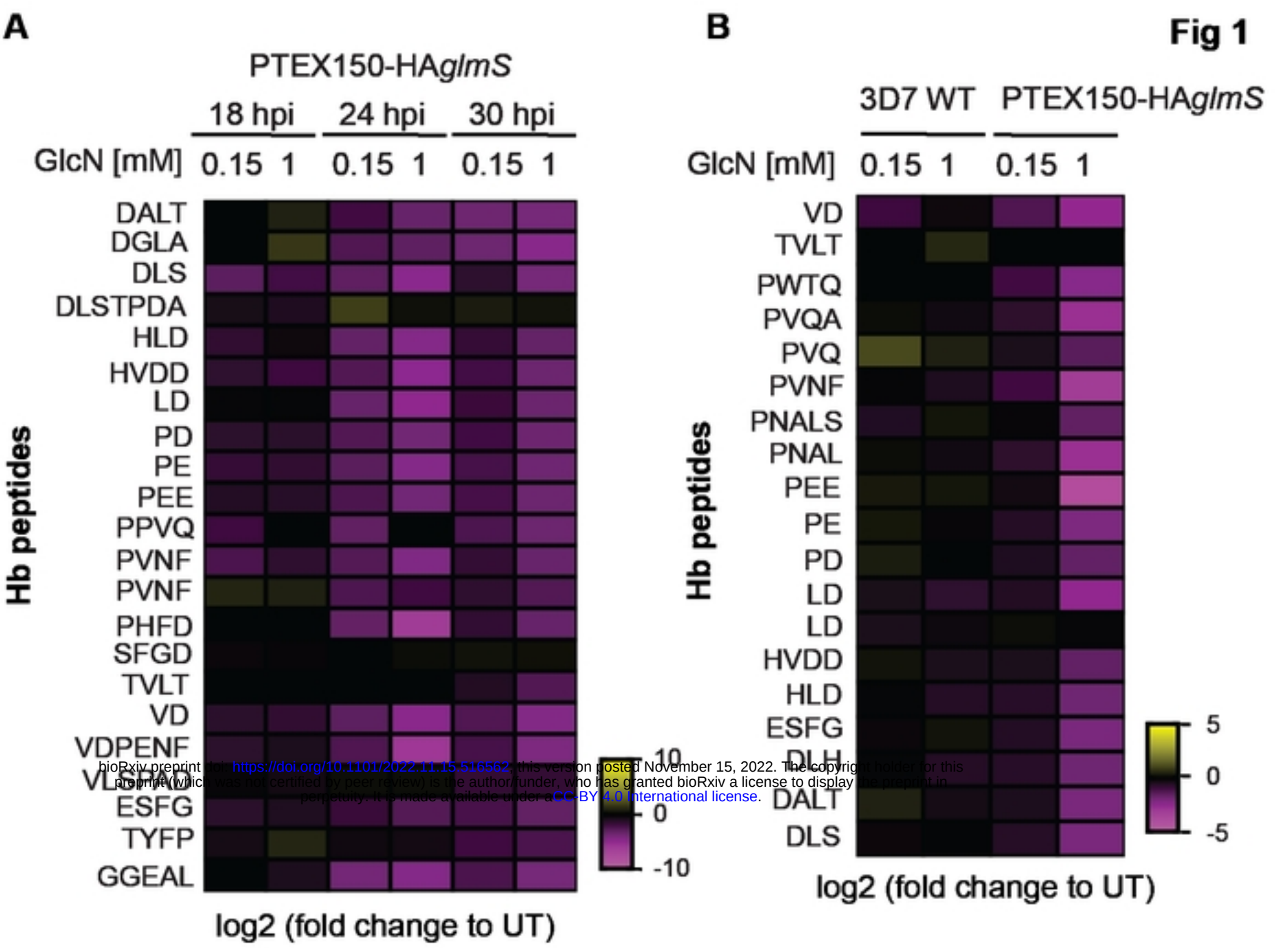

Figure 1

Figure 2

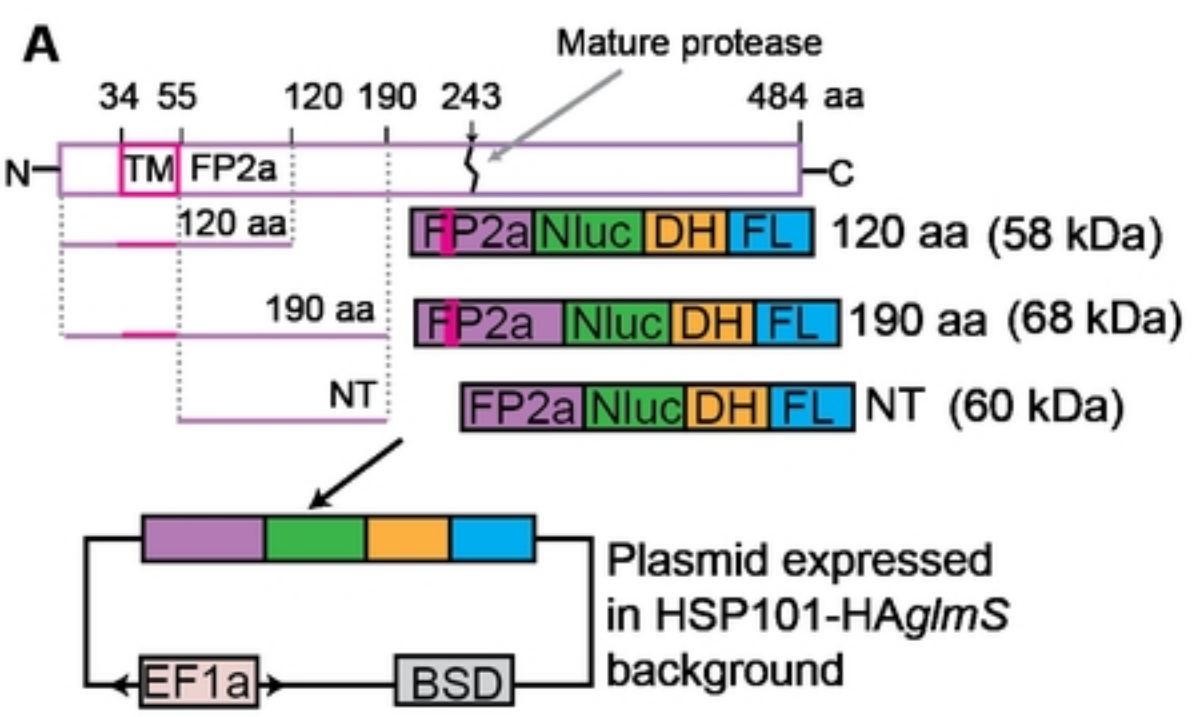

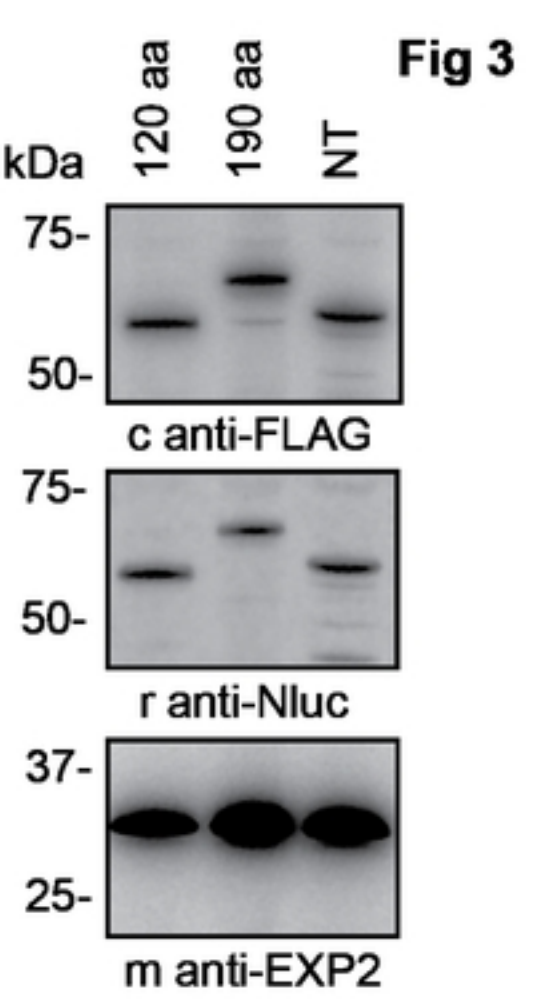

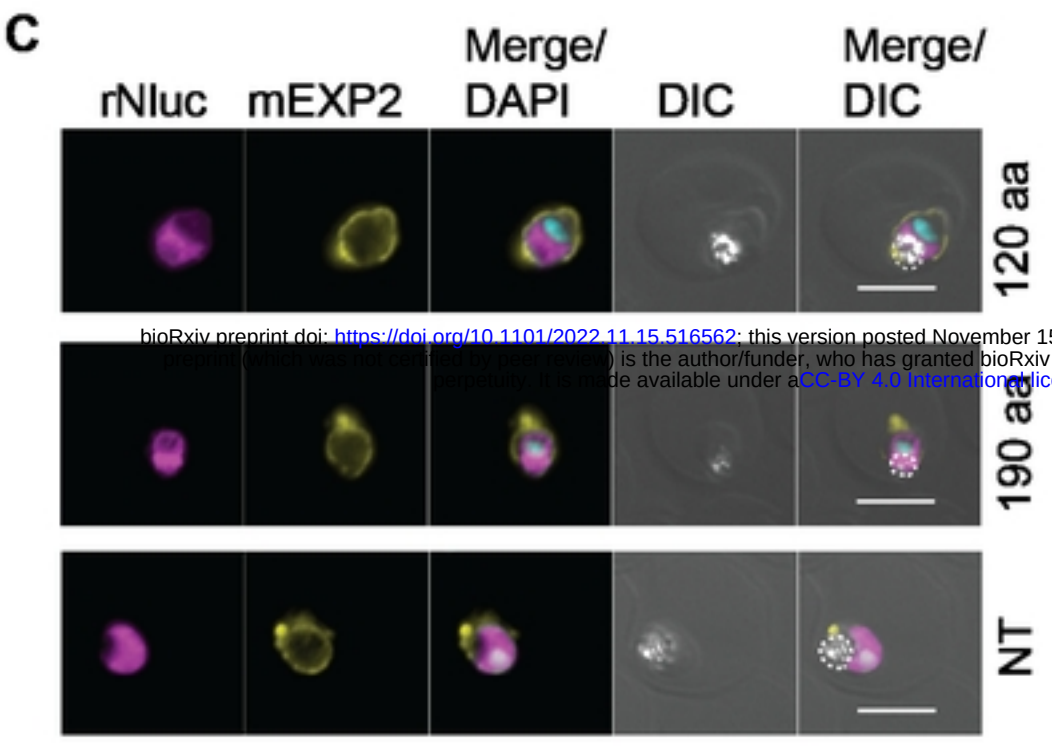

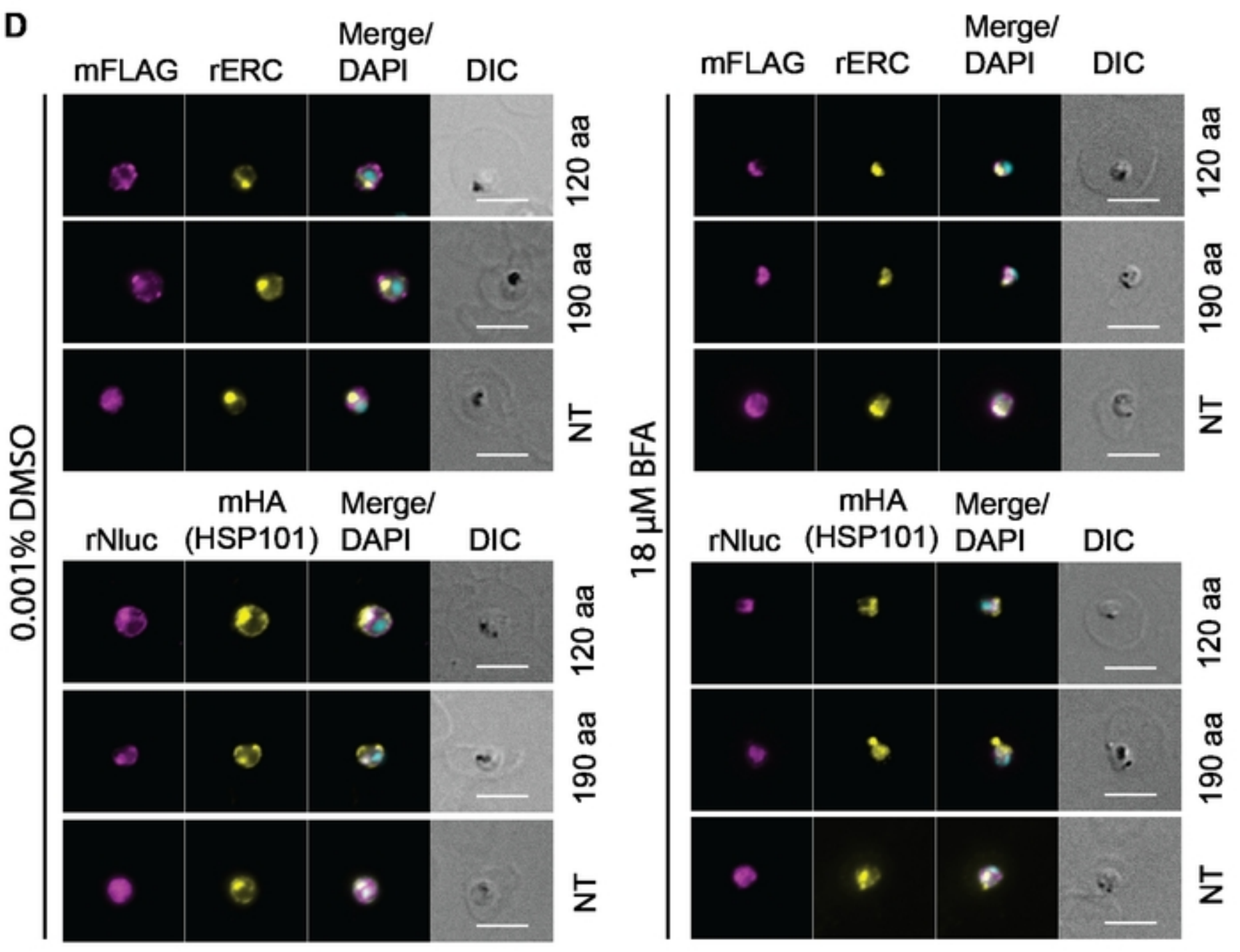

Figure 3

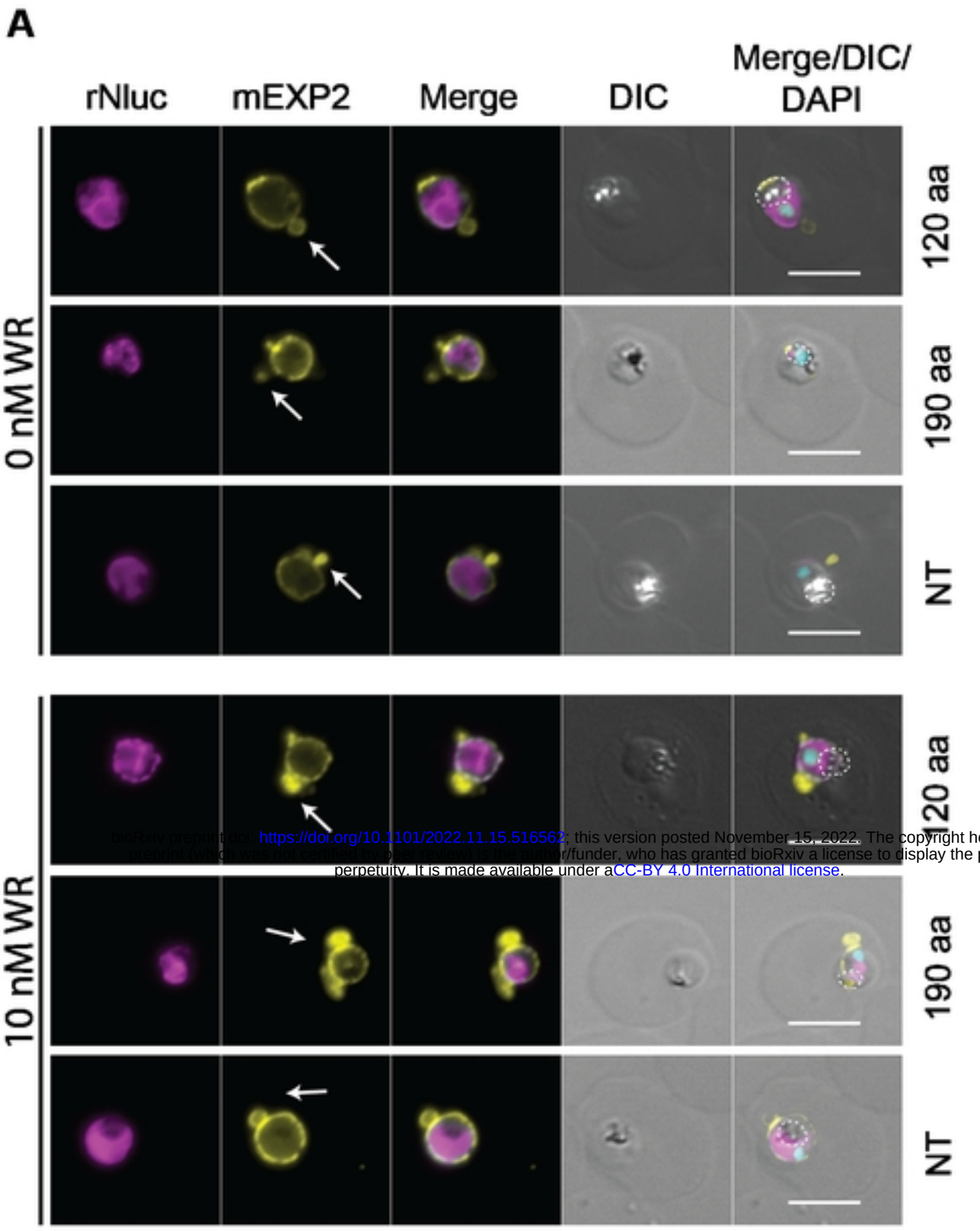

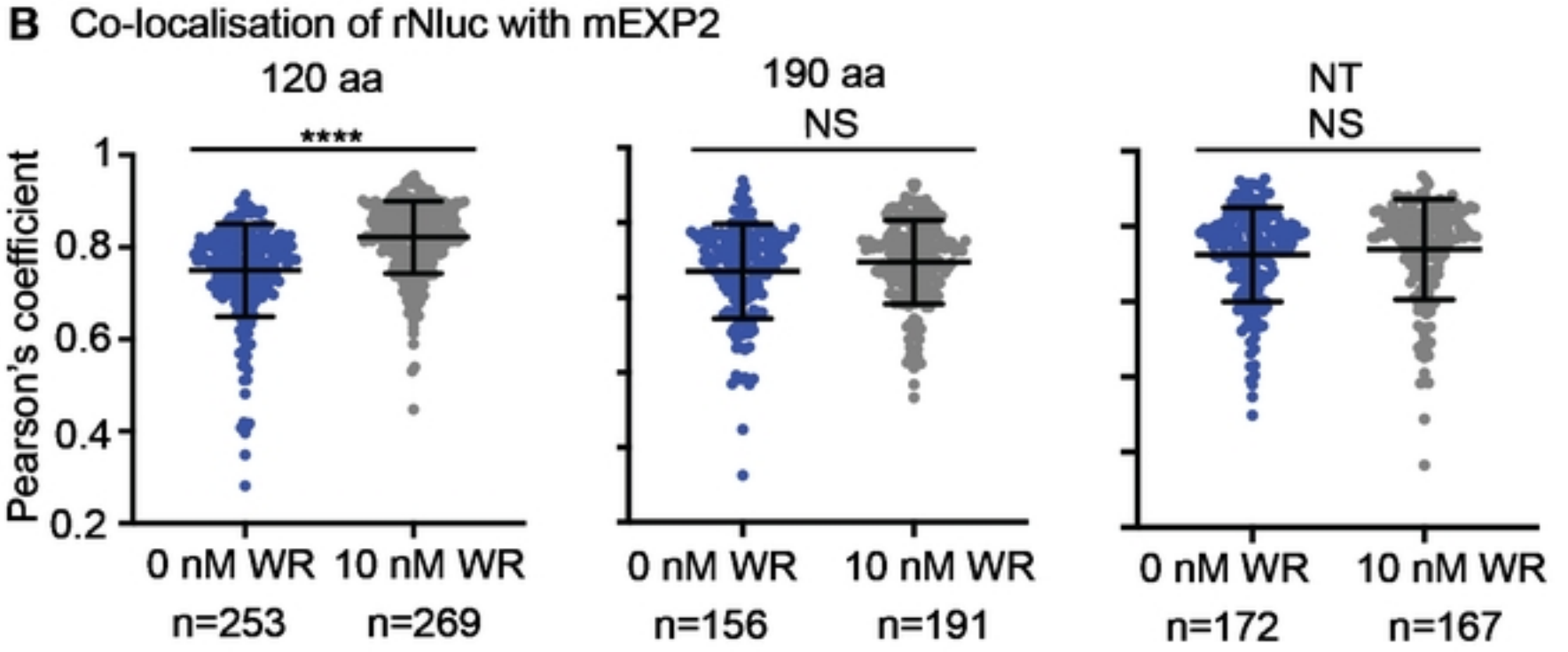

Figure 4

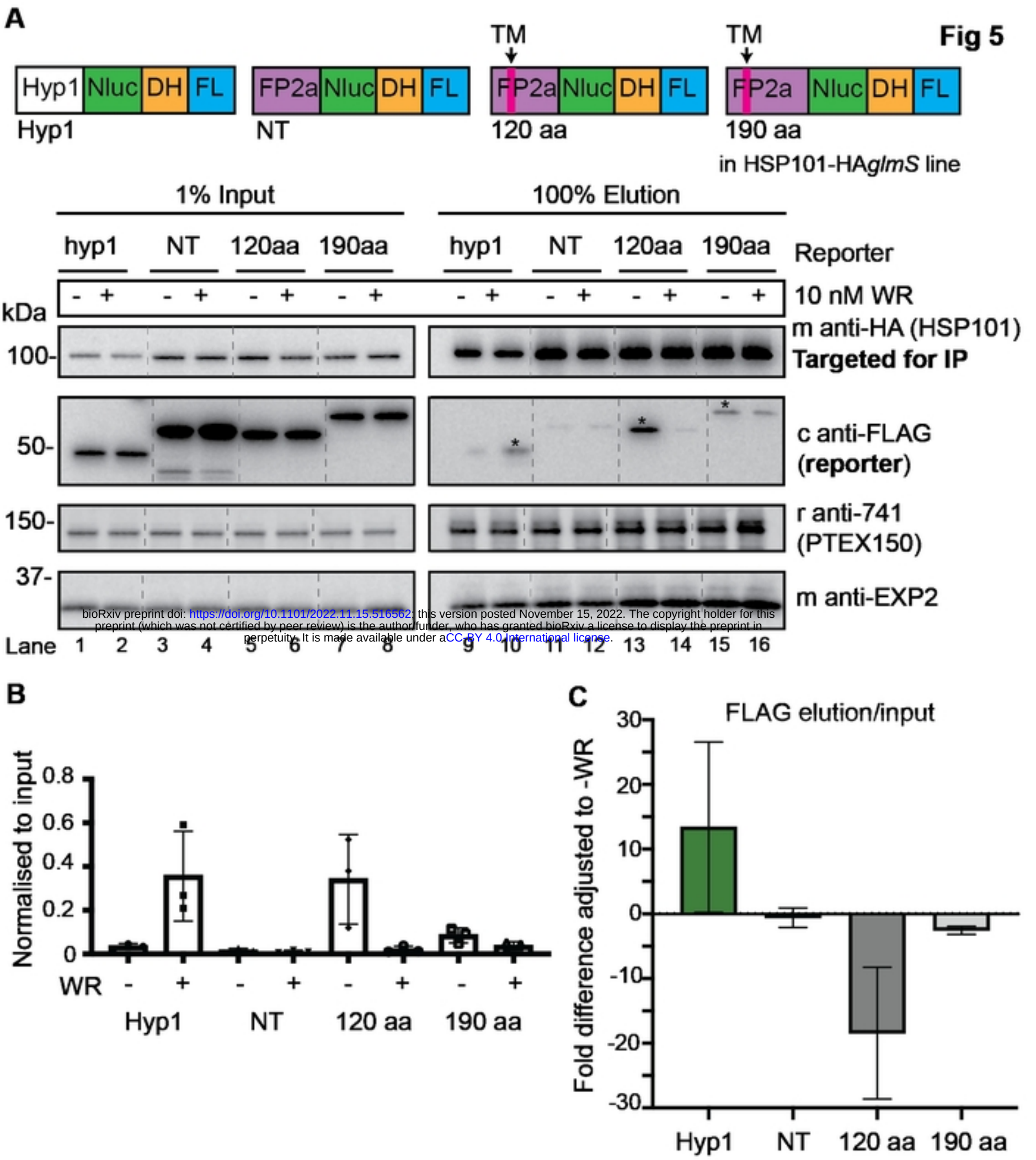

Figure 5

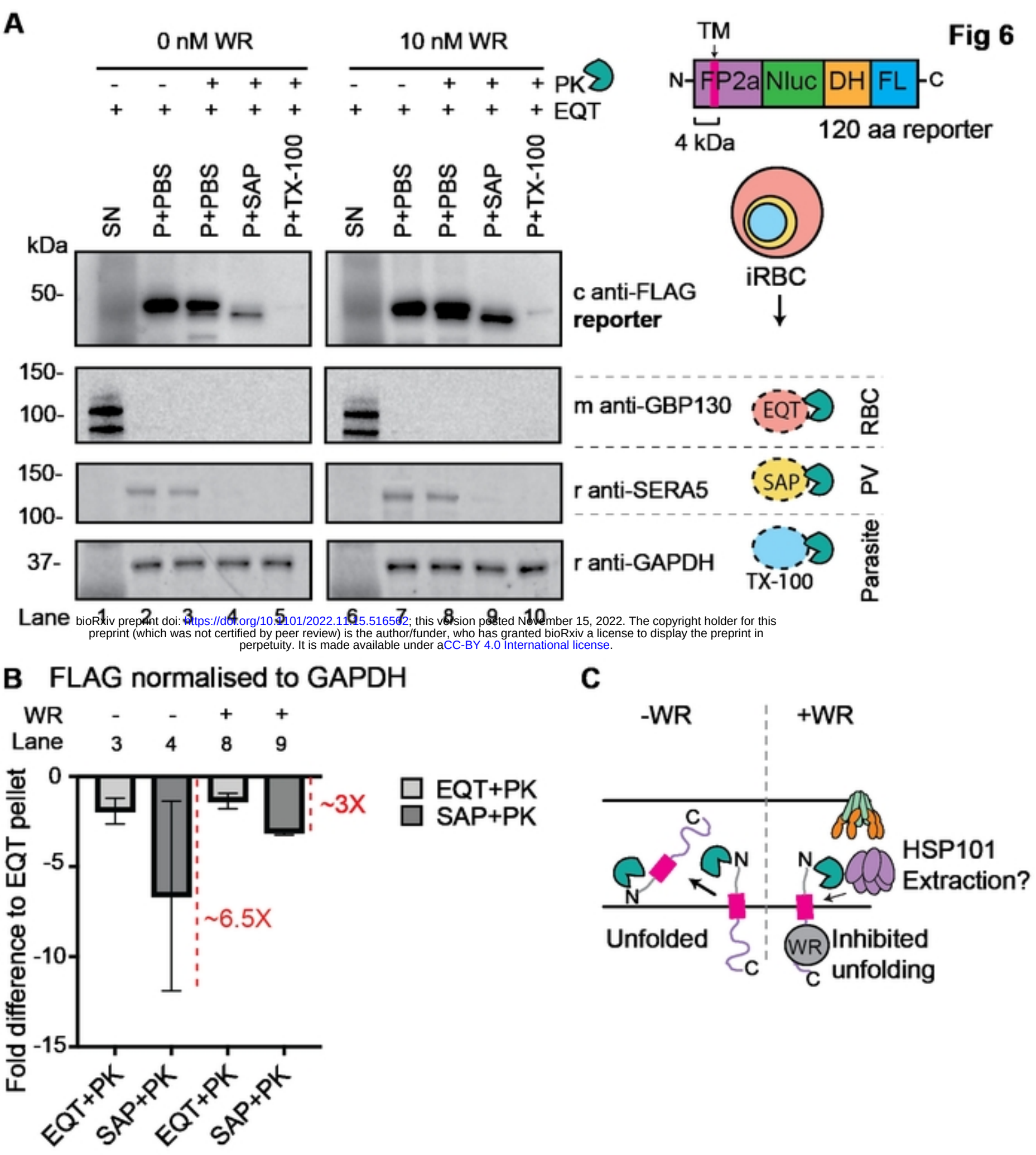

Figure 6

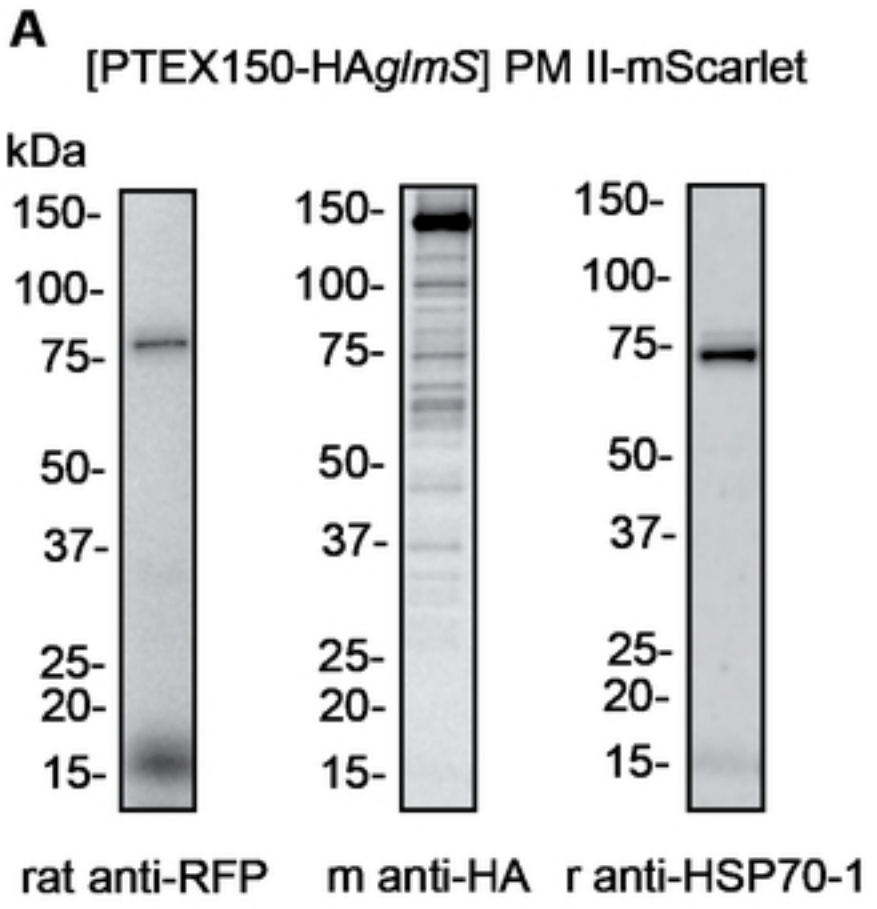

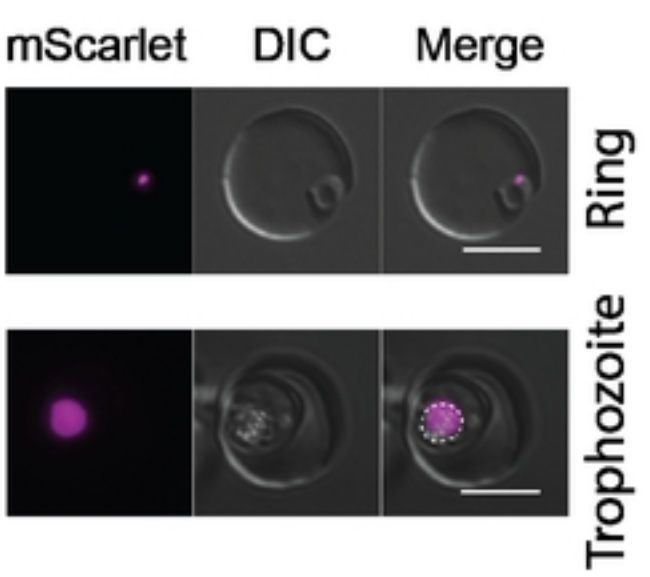

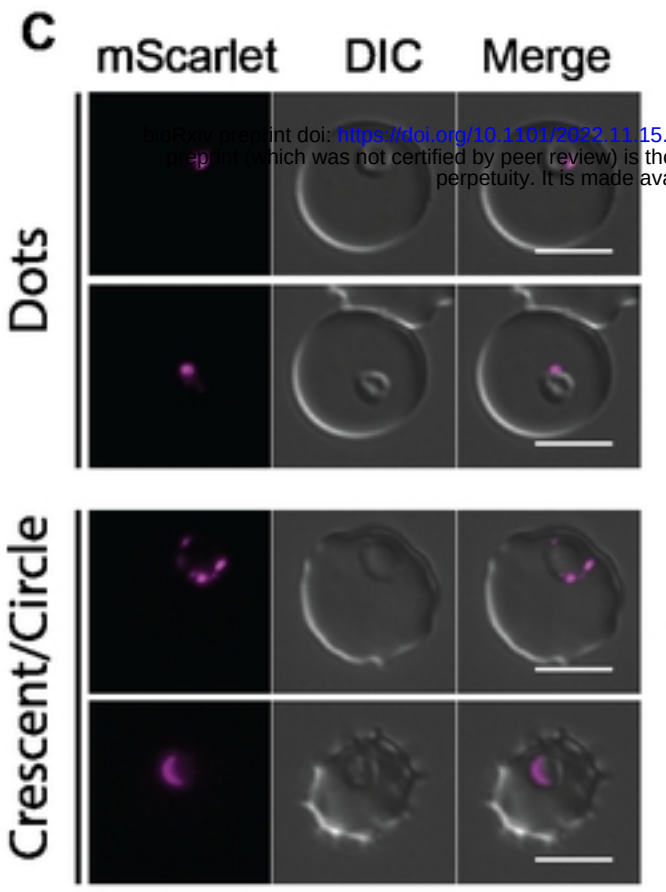

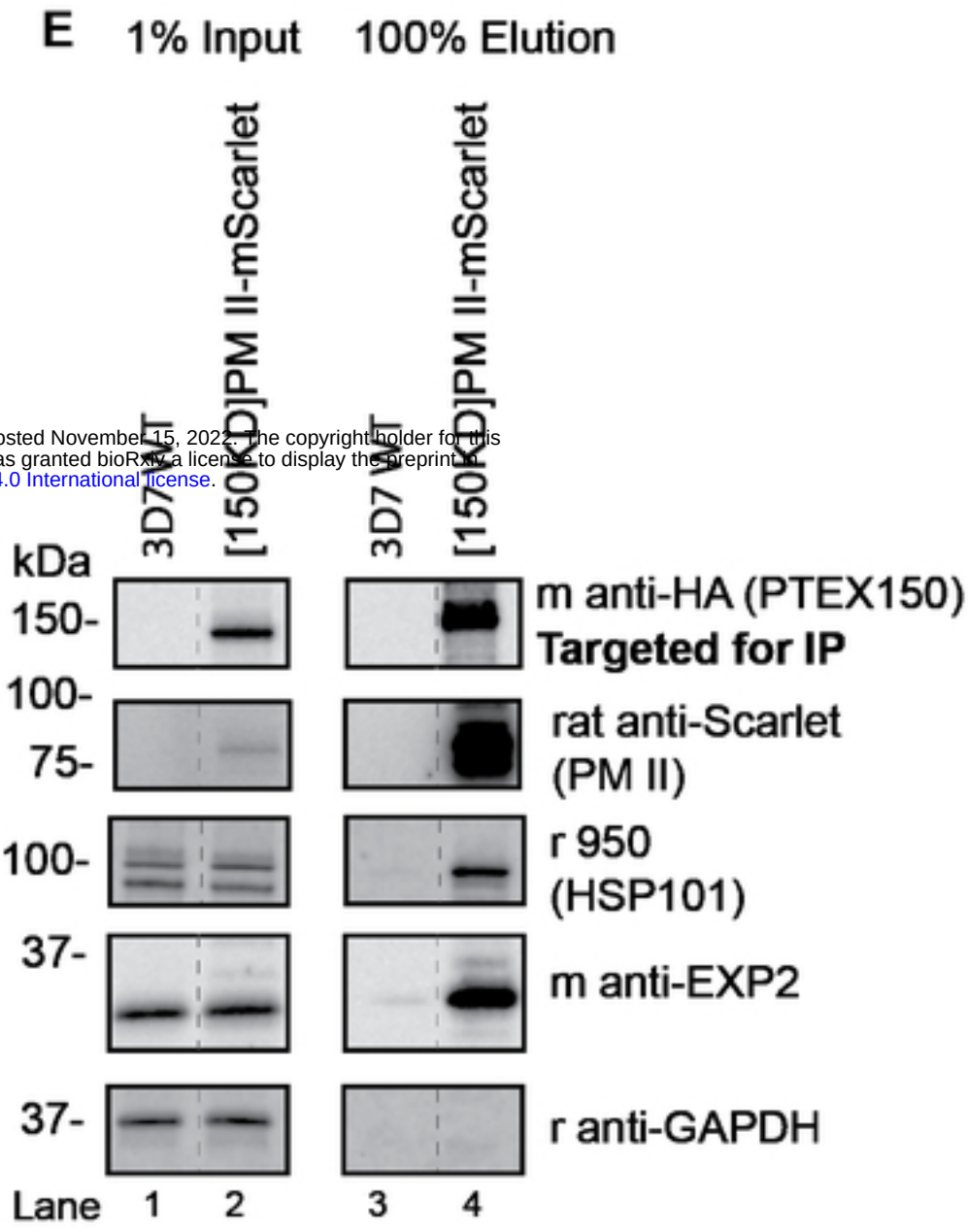

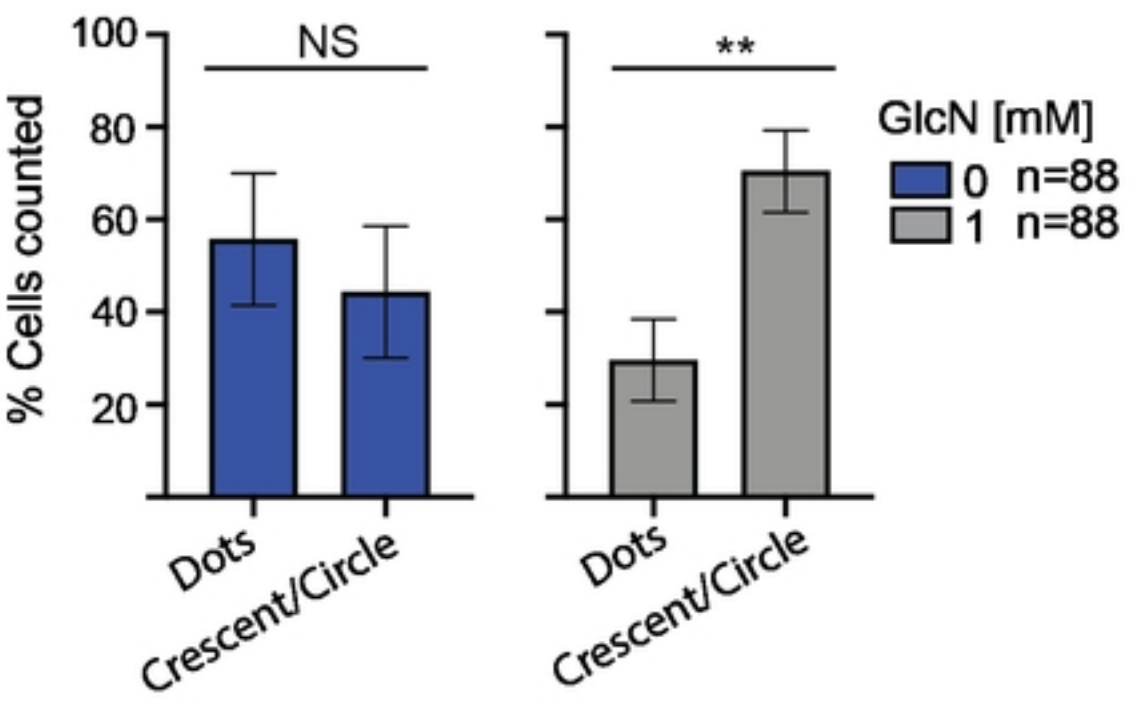

Figure 7

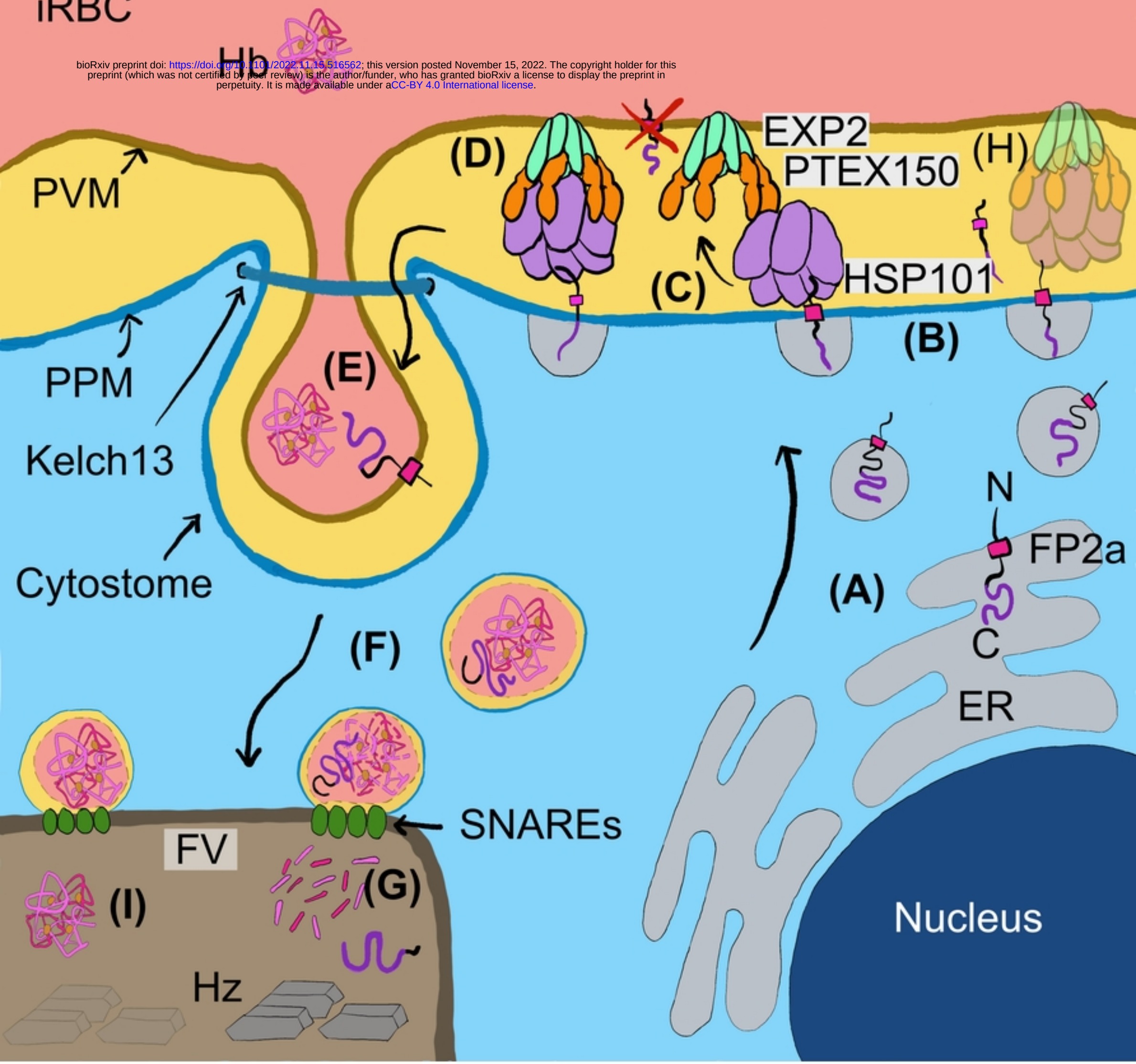

Figure 8